Università di Napoli
"Federico II"

National Quantum Science and Technology Institute

High-Q cavity coupled to a high permittivity dielectric resonator for sensing applications

Antonio Cassinese

Dept. of Physics, Università di Napoli Federico II.

https://arxiv.org/abs/2410.05831

Shahnam Gorgi Zadeh, CERN, Alberto Ghirri, CNR NANO, Sergio Pagano, Univ. Of Salerno, Simone Tocci, Claudio Gatti, INFN- LNF and Antonio Cassinese Univ. Napoli Federico II

QT4HEP- Workshop 20-24 January 2025

Hiqh microwave resonator Period: 1994 -2002

Dielectric resonators f=9 and19 Ghz

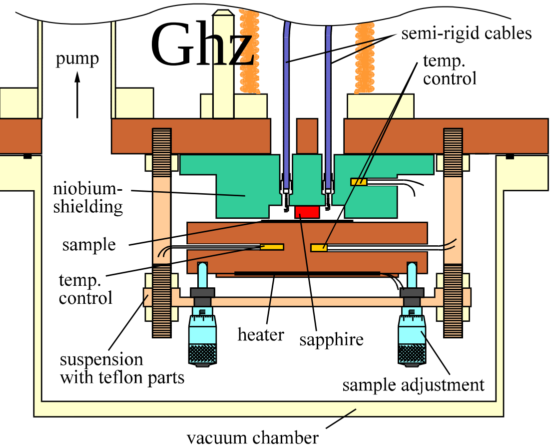

T. Kaiser, *et al.* ,Particle Accelerators **60**, 171 (1998).

Univ. Wuppertal

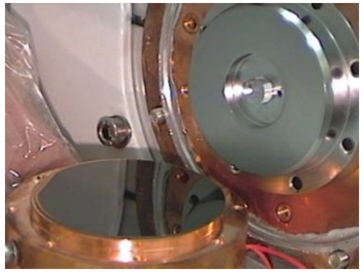

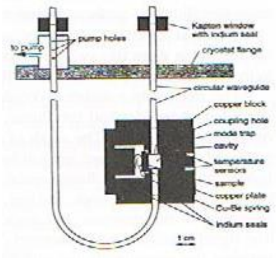

End wall cavity 87 Ghz

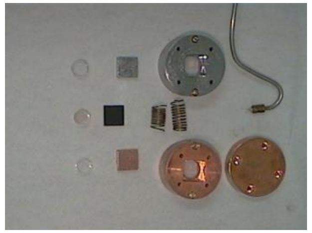

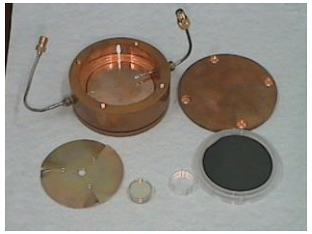

Microstrip resonator f=1,5-5 Ghz

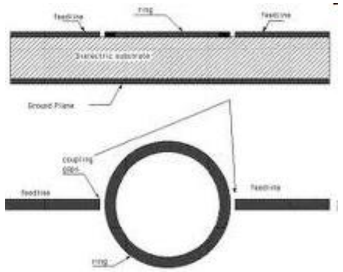

ring

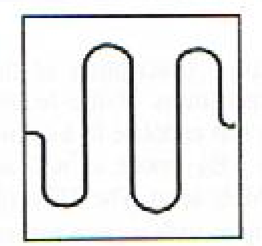

Meander

Superconducting cavities
f=1,5GHz (CERN, INFN- LNL)

Progetto Finalizzato CERN-INFN

Nb or Cu/Nb 1.5 Ghz single cell

Phd thesis 1995

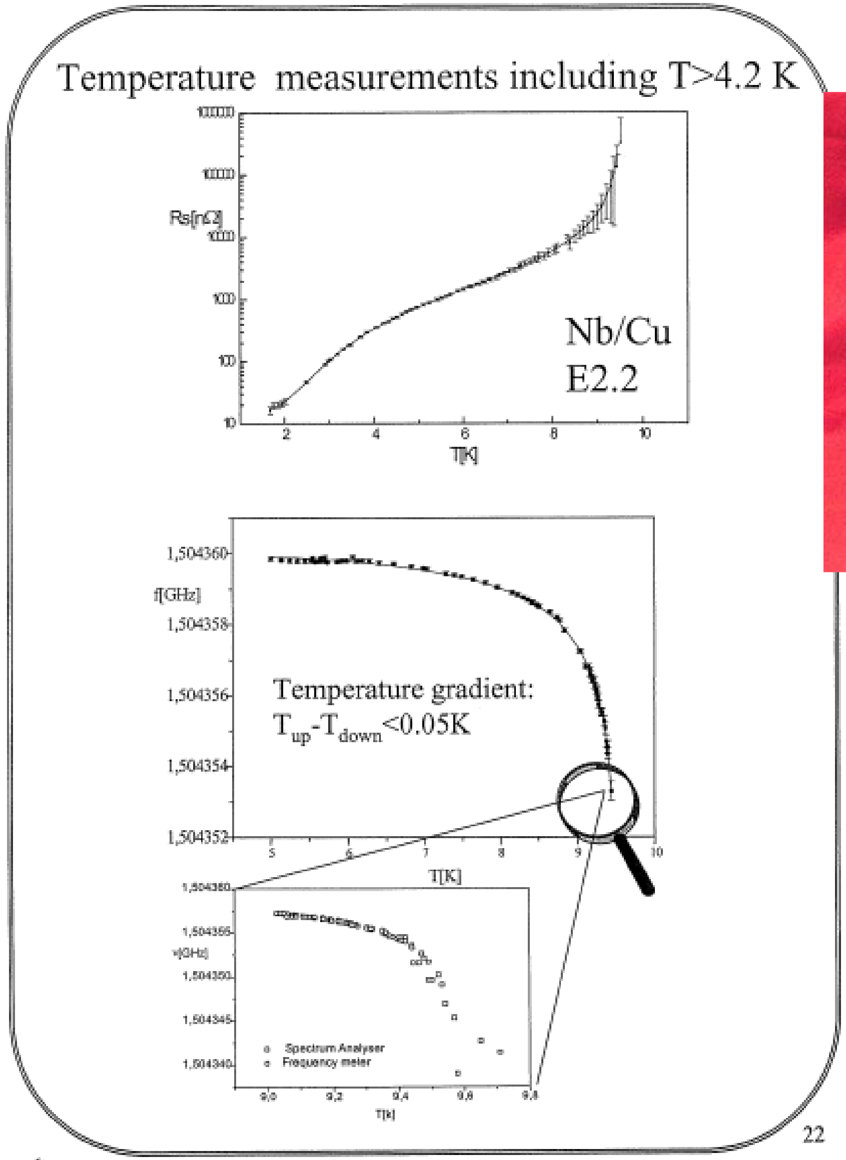

A. Cassinese

INFN ELOISATRON PROJECT, 38th Workshop:
Superconducting Materials for High Energy Colliders, Erice, 1999

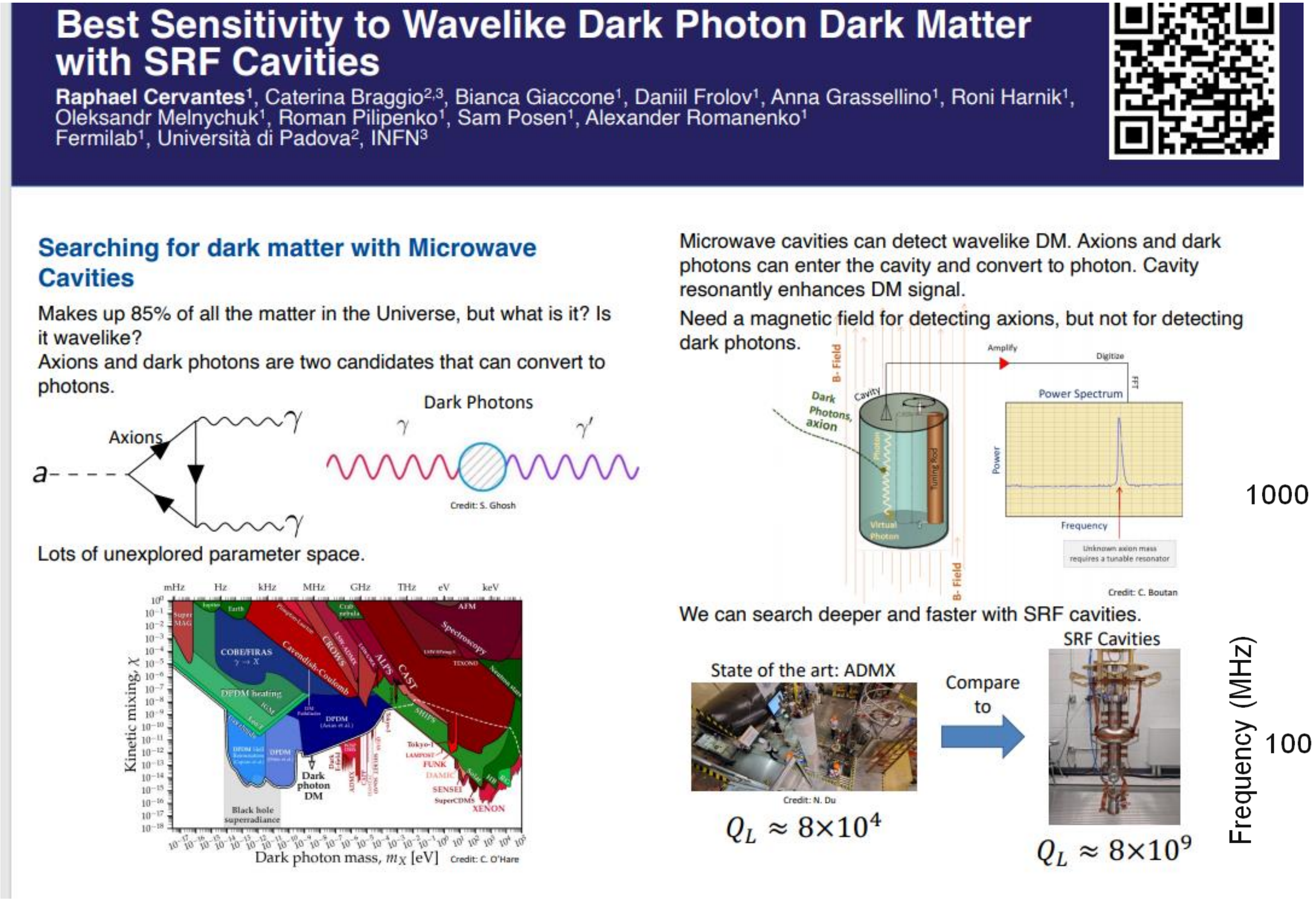

Already Existing cavities :

Choose Cavity Geometry to Match Particle Speed

β = *v/c* values

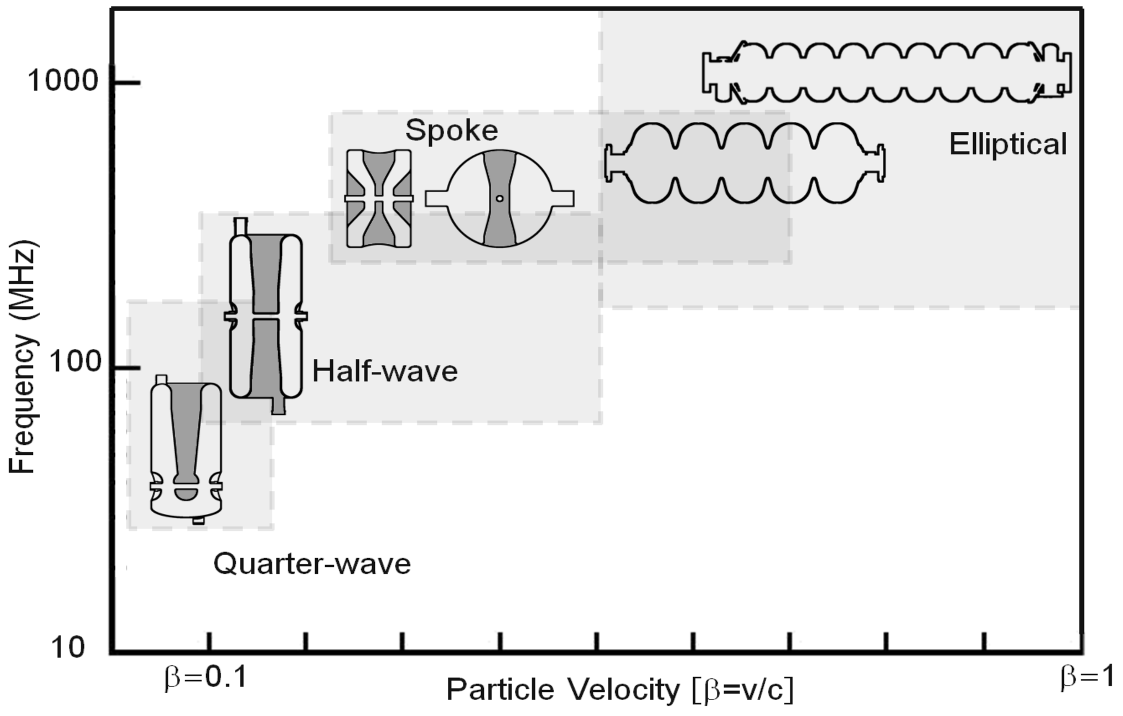

New Exclusion Limit for Dark Photons from an SRF Cavity-Based Search (Dark SRF)

A. Romanenko,[1,*] R. Harnik,[1,†] A. Grassellino,[1,‡] R. Pilipenko,[1] Y. Pischalnikov,[1] Z. Liu,[2,§] O. S. Melnychuk,[1] B. Giaccone,[1] O. Pronitchev,[1] T. Khabiboulline,[1] D. Frolov,[1] S. Posen,[1] A. Berlin,[1] and A. Hook[3]

[1] *Fermi National Accelerator Laboratory, Batavia, IL 60510, USA*
[2] *School of Physics and Astronomy, University of Minnesota, Minneapolis, MN 55455, USA*
[3] *Maryland Center for Fundamental Physics, University of Maryland, College Park, MD 20742*

(Dated: January 30, 2023)

arXiv:2301.11512v1 [hep-ex] 27 Jan 2023

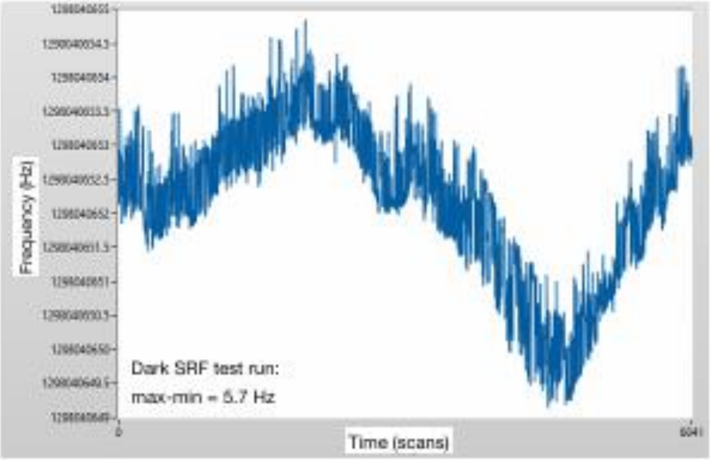

FIG. 2. The Dark SRF emitter frequency collected over 6041 scans (each lasting about a second). The frequency variation in this test spans 5.7 Hz. The emitter cavity was the less stable of the emitter-receiver pair.

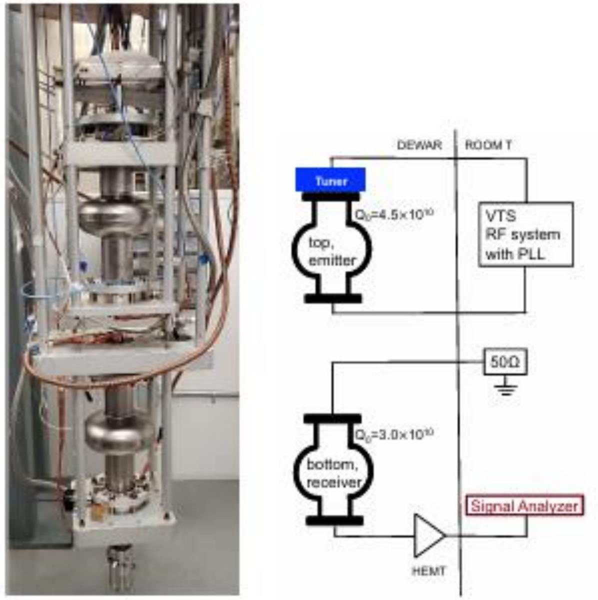

FIG. 1. Left: The experimental setup for the Dark SRF experiment consisting of two 1.3 GHz cavities. Right: A sketch of the Dark SRF electronic system.

19th Int. Conf. on RF Superconductivity SRF2019, Dresden, Germany JACoW Publishing
ISBN: 978-3-95450-211-0 doi:10.18429/JACoW-SRF2019-TUP085

e work, publisher, and DOI.

OPERATION OF AN SRF CAVITY TUNER SUBMERGED INTO LIQUID HELIUM*

Y. Pischalnikov†, D. Bice, A. Grassellino, T. Khabiboulline, O. Melnychuk, R. Pilipenko, S. Posen, O. Pronichev, A. Romanenko, Fermi National Accelerator Laboratory, Batavia, IL, USA

Level of the microphonics on the single cell 1.3 GHz cavity, installed at FNAL VTS facility, was ~3 Hz (rms). Main resonances were in the range of 20-50 Hz. Using piezo-tuner with active compensation could suppress microphonics below rms = 1 Hz [5].

Minimum-to-maximum frequency variation in this run was 3Hz.

Coherent coupling between molecular spin ensembles and high critical temperature superconducting coplanar resonators ($\geq$ 2016)

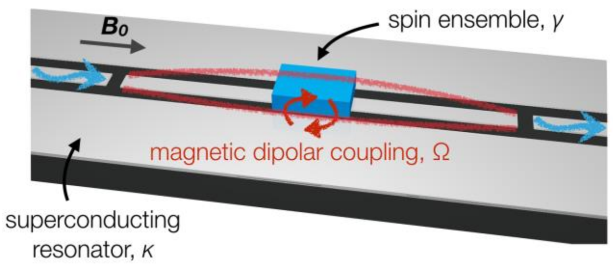

$$\Omega = g_{\text{eff}} \frac{\mu_B}{h} \sqrt{n \int_V \left| \langle G | \vec{b}_{\text{rms}} \cdot \vec{S} | E \rangle \right|^2 dV}$$

Strong coupling regime: $\Omega \gg \gamma, \kappa$

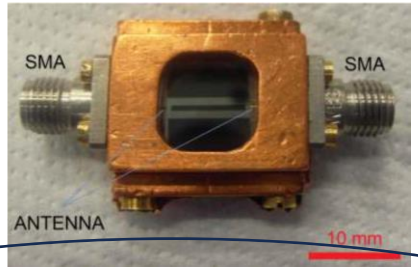

Uni Modena-CNR NANO

Bare resonator

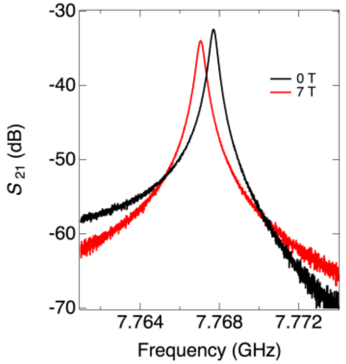

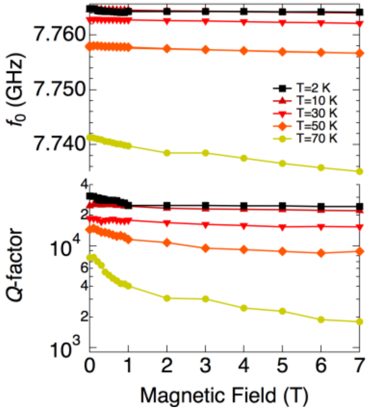

- Q-factor > 10^4 at 2 K
- Wide temperature range (Tc=87 K)
- Stable in applied magnetic field up to 7 T (in-plane) and 1 T (out-of-plane)
- High critical current density

Appl. Phys. Lett. 106, 184101 (2015)

Strong coupling with ensembles of organic radical spins

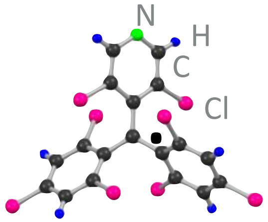

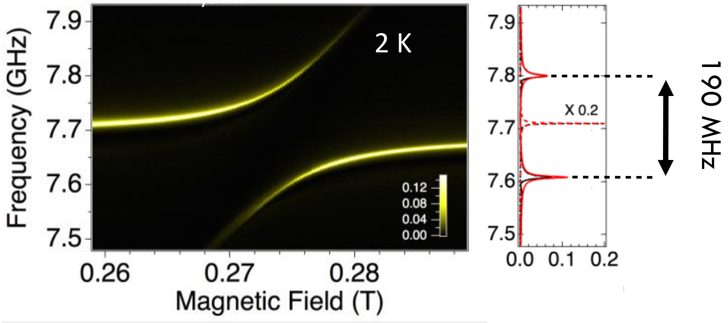

We report the evolution of the transmission peak in correspondence to the resonance field of the DPPH spin ensemble (Br=0.276 T). At 2 K, two branches are observed, which indicate the presence of a large anticrossing between the resonator mode and the spin ensemble

Radicals synthesized
by L. Beverina (Uni. Milano Bicocca)

Phys. Rev. A 93, 063855 (2016)

We grew a single-crystal of pentance:*p*-terphenyl

After investigating a fullerene derivate, we stumbled upon a pentacene which had a **huge** EPR signal

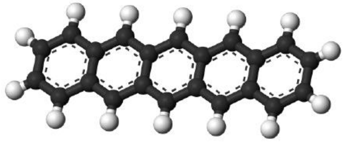

Pentacene

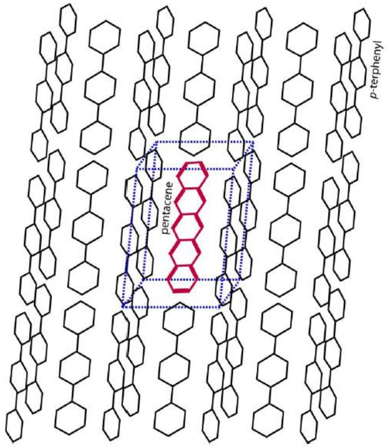

Alford Group , Imperial college

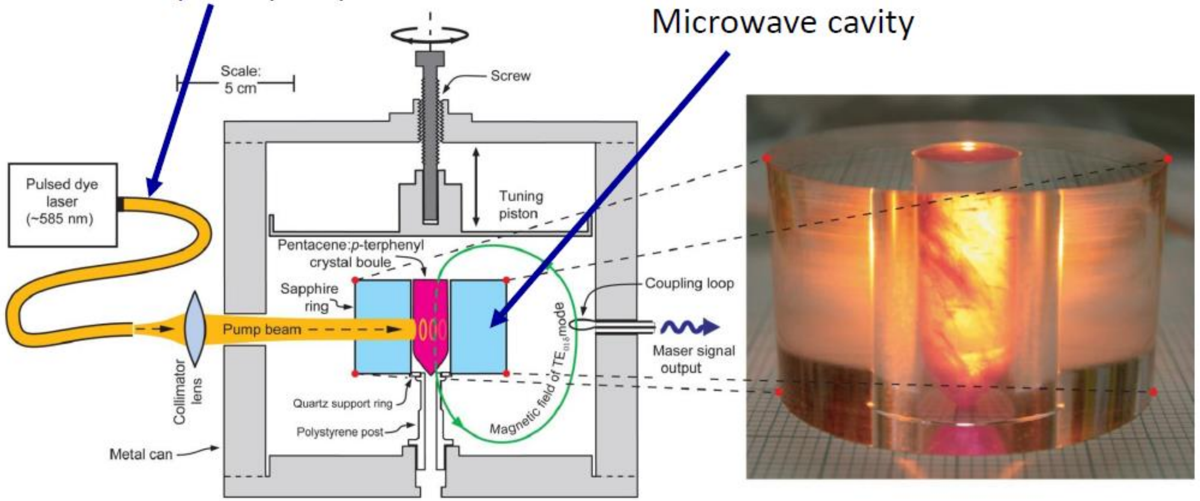

Pumping scheme for pentacene-doped *p*-terp

"triplet mechanism" (TM)

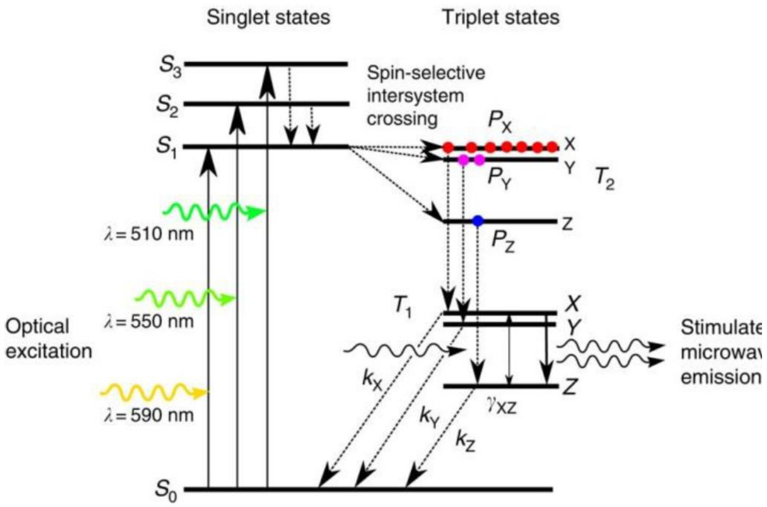

Maser Response to nanosecond laser

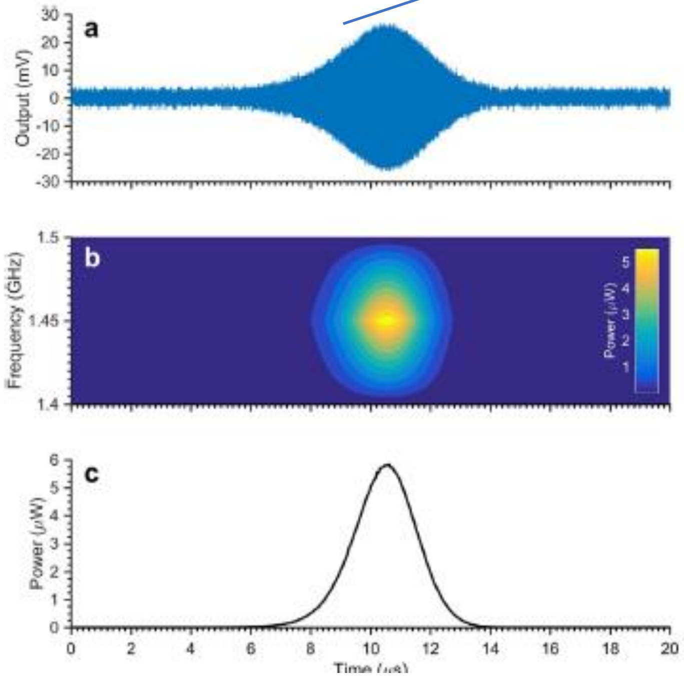

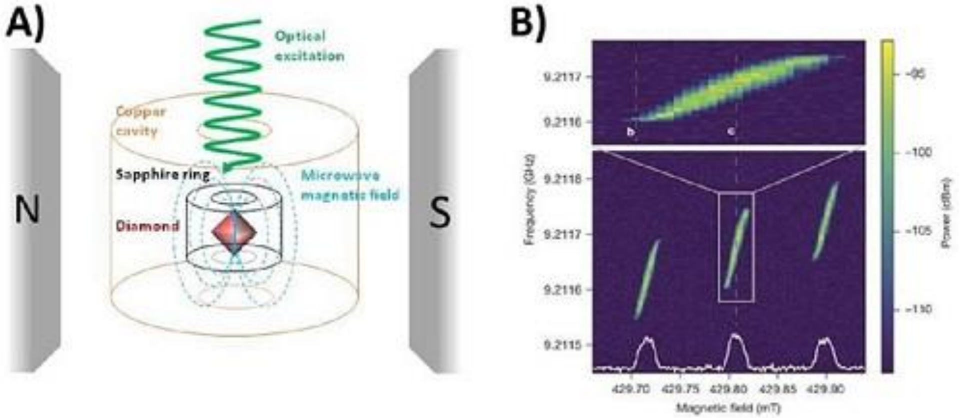

Figure 1 A) Schematic description of the experimental apparatus used to achieve maser action with a 3D diamond. **B)** Maser emission (spectral power in colour scale) as a function of the applied magnetic field. The three peaks correspond to the hyperfine lines due to the nitrogen nucleus (*I* = 1). Figure taken and adapted from reference [9].

Possible Maser gain media – Picene & Pentacene (PRIN submitted 2020)

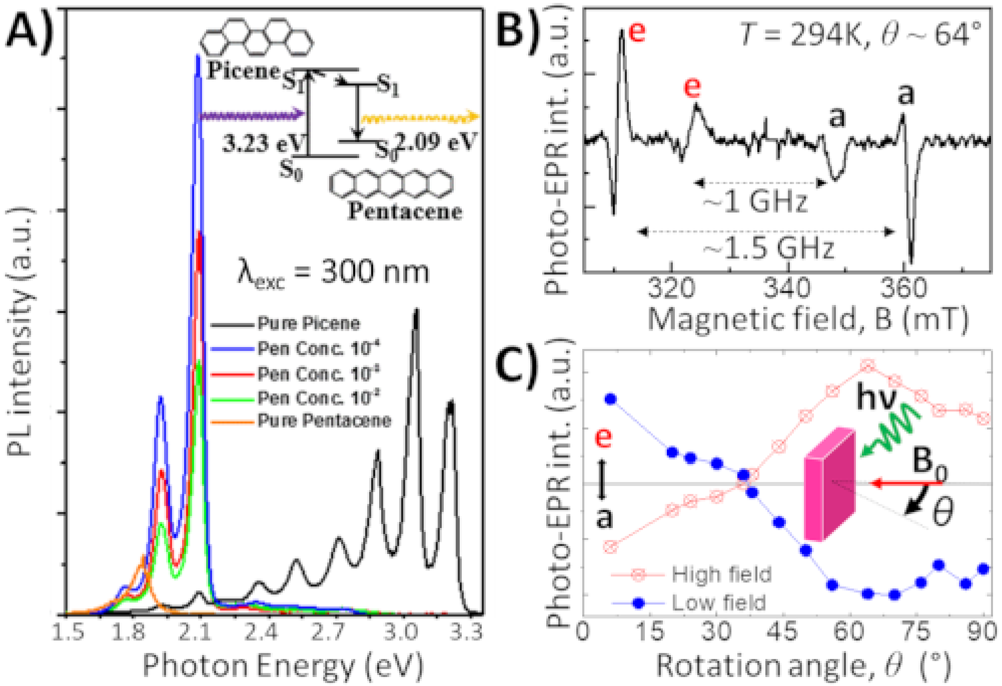

Figure 2 A) PL spectra of pentacene in picene with different concentrations. Inset: molecular energy levels. **B)** Photo-EPR spectrum of a picene doped pentacene single crystal. **C)** Angular dependence of the resonance line intensities. Inset: sketch of the experimental geometry.

Adsorption spectra of Picene and Picene doped Pentacene increasing pentacene percentage. The presence of pentacene change dramatically the PL spectra. The Picene bands vanish while new bands due to single pentacene emission appears.

EPR In dark (F. Moro UNI Bicocca)

Picene+penatcene Crystals <1%

Journal of Materials Research
2022-03-28 DOI: 10.1557/s43578-022-00536-y

Collaboration
Uni- Bicocca
Uni-To
Uni Modena- CNR Nano
Uni Napoli –CNR SPIN
CNR IMEM

J. Phys. Chem. C, **2018**, 122 (29), pp 16879–16886

A single resonance was observed in dark On crystal Picene/pentacene

g-value= 2.002

FWHM = 4 G

No orientation dependence

Other materials considered
Diamond with NV 2.1 Ghz

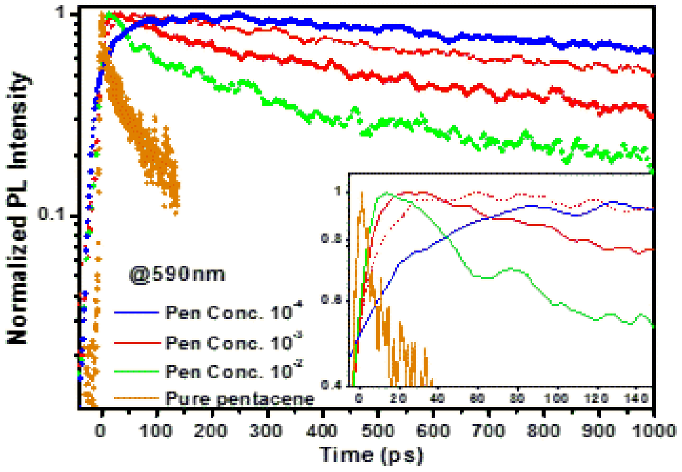

Planar resonator of interest for 2D MASER

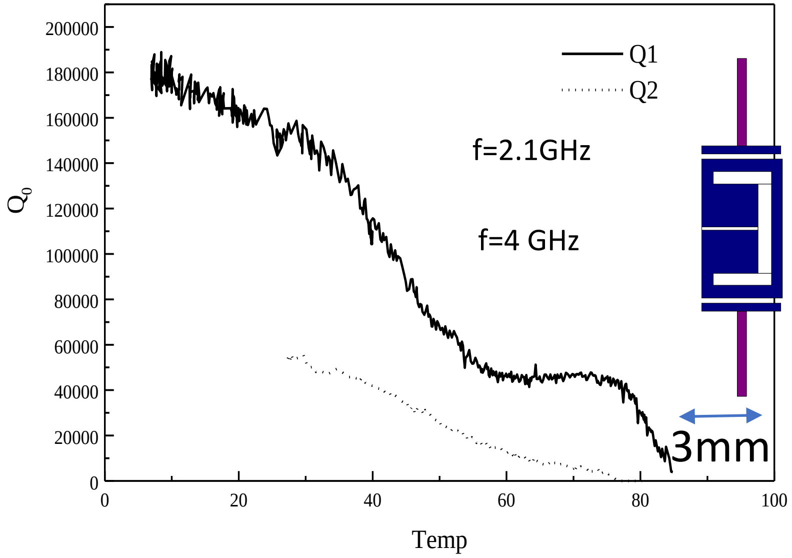

MICROW. AND OPT. TECH. LETT. / Vol. 35, No. 5, 360, 2002
In collaboration with james cook university Australia

Coupled Resonator Calorimeter for Particle Detection

Ling Hao, Giuseppe Lorusso and John Gallop

National Physical Laboratory, Hampton Road, Teddington TW11 0LW, UK

Corresponding author: ling.hao@npl.co.uk

Citation information: DOI 10.1109/TIM.2021.3062171, IEEE

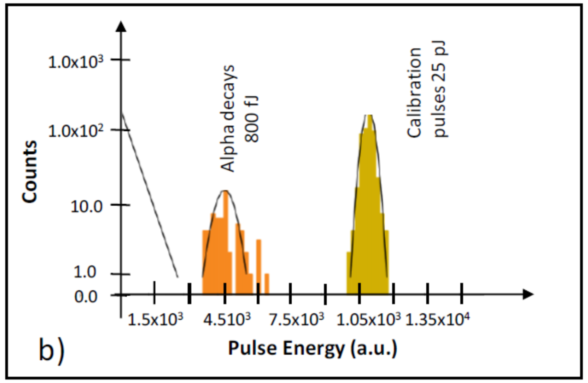

Fig. 8 a) A 2s trace of events, including one alpha decay and two calibration pulses b) A histogram of 80 alpha decays and 400 calibration pulses (each ~ 1ms duration).

$$\Delta T^2 = \frac{k_B T^2}{C} \quad .....(1)$$

Thus the single photon coupling strength G becomes

$$G = \frac{df}{dT}\Delta T = T\frac{df}{dT}\left(\frac{k_B}{C}\right)^{\frac{1}{2}} \quad .....(2)$$

$E \sim$ 10^{-23} J/Hz @ 1K

10^{-20} J/Hz @ 10K

2.5×10^{-19} J/Hz @

fitted by the above equations and that the rate of change of resonant frequency with temperature $df(T)/dT$ can be as high as 75 MHz/K. Since the output frequency of a microwave loop oscillator based on a modestly high Q dielectric resonator can be stable to at least 1 in 10^{11} for an averaging time of 1 s [3], the thermometer has a potential resolution of at least 1.5 nK,

$$\delta E = \frac{2C}{f(\frac{d\varepsilon}{\varepsilon dT})T} \quad .....(3)$$

Using an approximate analytical form for the temperature dependence of $\varepsilon_r(\mathrm{STO}) = \varepsilon'/T$, (where $\varepsilon' \sim 10^5$) which is valid for the temperature range between about 20–80 K, we can differ-

$$\left.\frac{df(T)}{dT}\right|_{\max} = \left[\frac{A}{(W_{\mathrm{STO}})^2}\frac{dg(T)}{dT}\right]. \qquad \frac{df(T)}{dT} = \frac{Af_0}{2W_{\mathrm{STO}}^2 T}.$$

$$\boldsymbol{\varepsilon(T) = \varepsilon_0 + \frac{C}{\frac{T_1}{2}\coth(\frac{T_1}{2T}) - T_0}}$$

Where:

- ***T* is temperature**
- ***C*, T_1 and T_0 are fitting parameters**

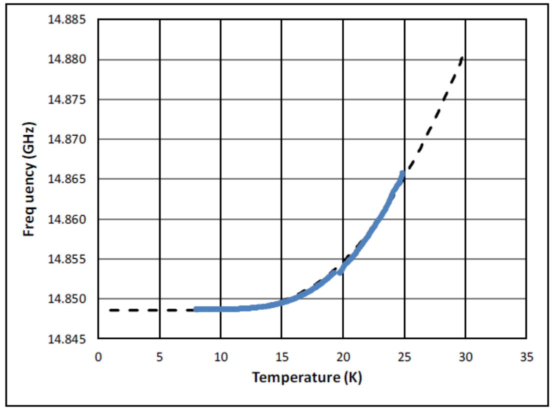

Fig. 6 Measured frequency shift of a coupled resonance at 14.87GHz, with best fit to equation (4), shown by the dashed line.

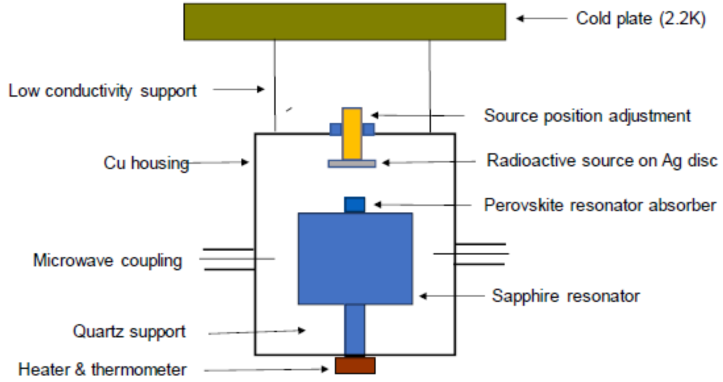

Fig. 3 Schematic layout of the coupled resonator system.

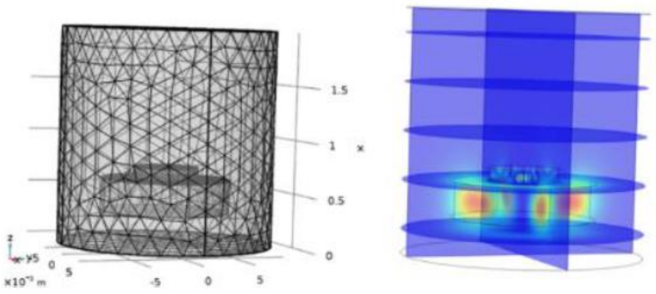

Fig. 2 COMSOL finite element model of the coupled resonator system for $SrTiO_3$ permittivity 650, f =11.426GHz with housing size 20 x 20 mm. a) Meshed geometry of the MCR system, b) Standing wave pattern of this coupled mode.

Applications of Coupled Dielectric Resonators Using $SrTiO_3$ Pucks: Tuneable Resonators and Novel Thermometry

John C. Gallop and Ling Hao

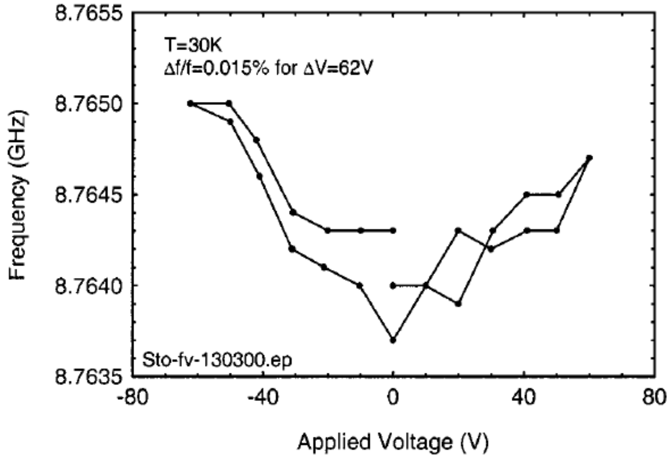

Fig. 4. Tuning effect of applied voltage to STO.

In Fig. 4, we show the effect of a modest applied electric field on the frequency of the loop oscillator. Note the total tuning range achieved is around 0.015% (1.5 MHz) for an applied voltage change of only 60 V. However, note also that there is some indication, at 30 K, of hysteresis in the frequency versus voltage plot.

Using an approximate analytical form for the temperature dependence of $\varepsilon_r(\mathrm{STO}) = \varepsilon'/T$, (where $\varepsilon' \sim 10^5$) which is valid for the temperature range between about 20–80 K, we can differ-

$$\frac{df(T)}{dT} = \frac{Af_0}{2W_{\mathrm{STO}}^2 T}.$$

Thus, it is important to operate with a mode overlap coupling between the resonators which is as strong as possible, with the loss tangent $(\tan\delta)$ of the STO as low as possible (to minimize W_{STO}) and the temperature T as low as possible. If all of these parameters are optimized, this thermometer has a potential temperature resolution of at least 1.5 nK, comparable

Ferroelectrics, 335:45–50, 2006
Copyright © Taylor & Francis Group, LLC
ISSN: 0015-0193 print / 1563-5112 online
DOI: 10.1080/00150190600689217

Taylor & Francis
Taylor & Francis Group

Frequency Dependence of Dielectric Constant of Strontium Titanate Films with Single-Crystal-Like Behavior

H. TAKASHIMA,[1,*] R. WANG,[1] B. PRIJAMBOEDI,[1] A. SHOJI,[1] AND M. ITOH[2]

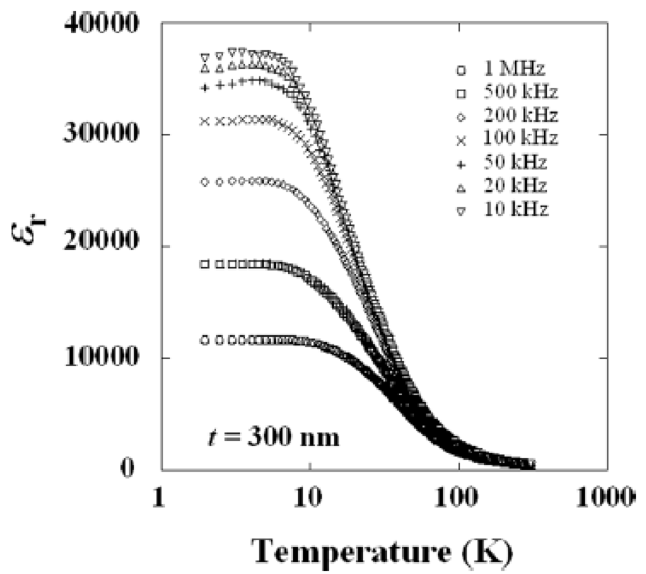

Figure 1. Temperature dependence of the dielectric constant at various frequencies for $SrTiO_3$ thin films with a thickness of 300 nm.

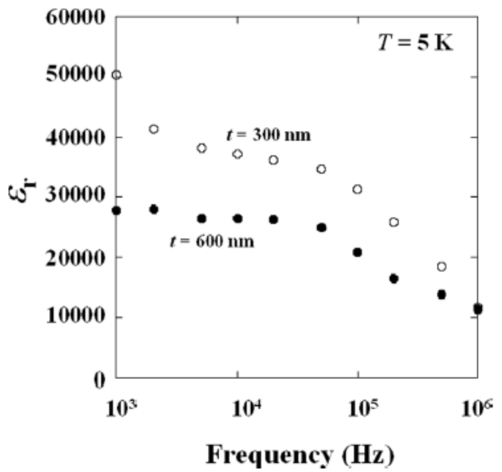

Figure 3. Frequency dependence of the dielectric constant at 5 K for $SrTiO_3$ thin films with 300 and 600 nm thickness.

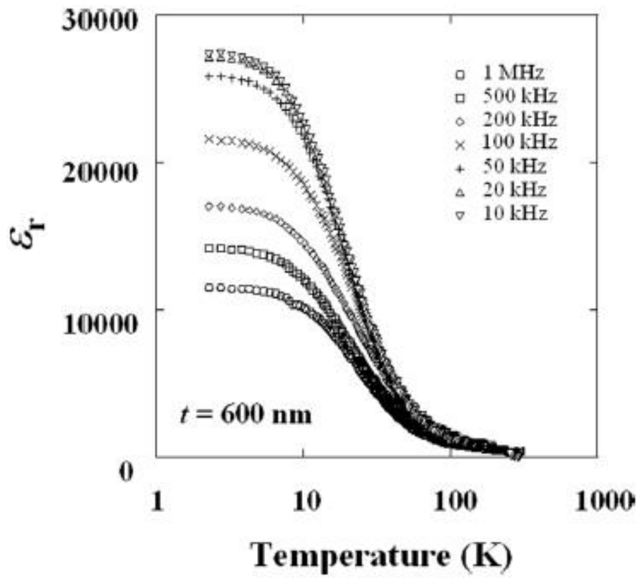

Figure 2. Temperature dependence of the dielectric constant at various frequencies for $SrTiO_3$ thin films with a thickness of 600 nm.

NATURE PHYSICS DOI: 10.1038/NPHYS4085

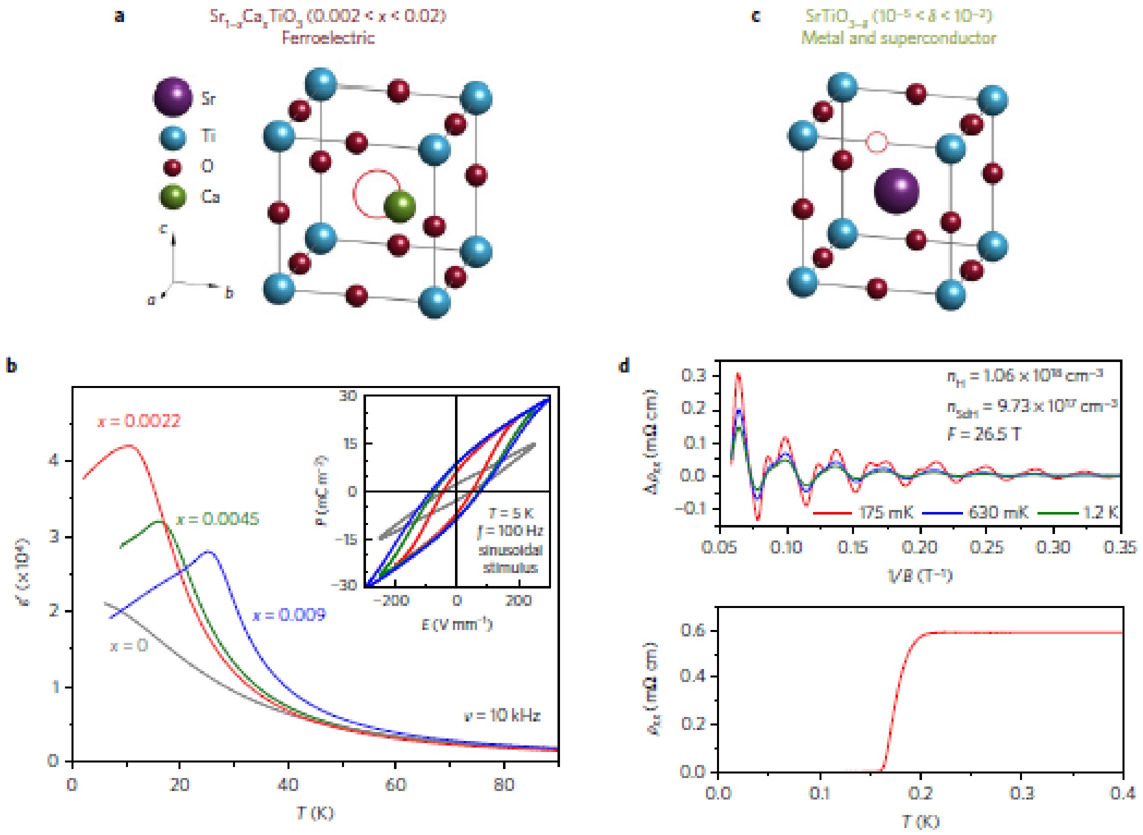

Figure 1 | Emergence of ferroelectricity and metallicity by atomic substitution in $SrTiO_3$. a, Substituting strontium with isovalent and smaller calcium atoms leads to ferroelectricity. Smaller calcium atoms can take off-centre positions and create local electric dipoles. Above a critical Ca threshold, a long-range ferroelectric order emerges below a Curie temperature. **b**, Ferroelectricity in insulating $Sr_{1-x}Ca_xTiO_3$ documented by the temperature dependence of the real component of the dielectric permittivity, ε', for three different x. The maximum in ε' marks the Curie temperature. The inset shows polarization–electric field hysteresis loops at $T = 5$ K. **c**, Removing an oxygen atom introduces two n-type carriers. **d**, Dilute metallic $SrTiO_3$ displays quantum oscillations of resistivity and a superconducting transition. The size of the Fermi surface according to the frequency of quantum oscillations (with period F) matches the carrier density (n) given by the Hall coefficient[5,6].

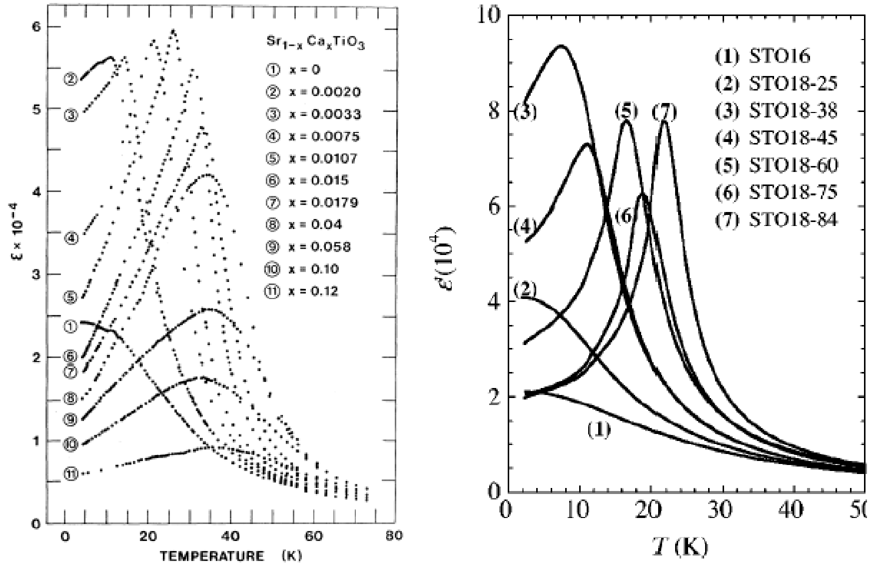

Figure 2.5: The temperature dependence of the dielectric constant during the ferroelectric transition. Left: for $Sr_{1-x}Ca_xTiO_3$ single crystals with $0 < x < 0.12$. Reproduced from[36] Right: for $SrTiO_3$ crystals substituted with ^{18}O isotope. Reproduced from[37]

Microwave Measurements on Superconducting Nb-Doped $SrTiO_3$

- Temperature dependence $\sigma_1(T)$ for certain frequencies
- Directly obtain values for superconducting gap $2\Delta(T)$

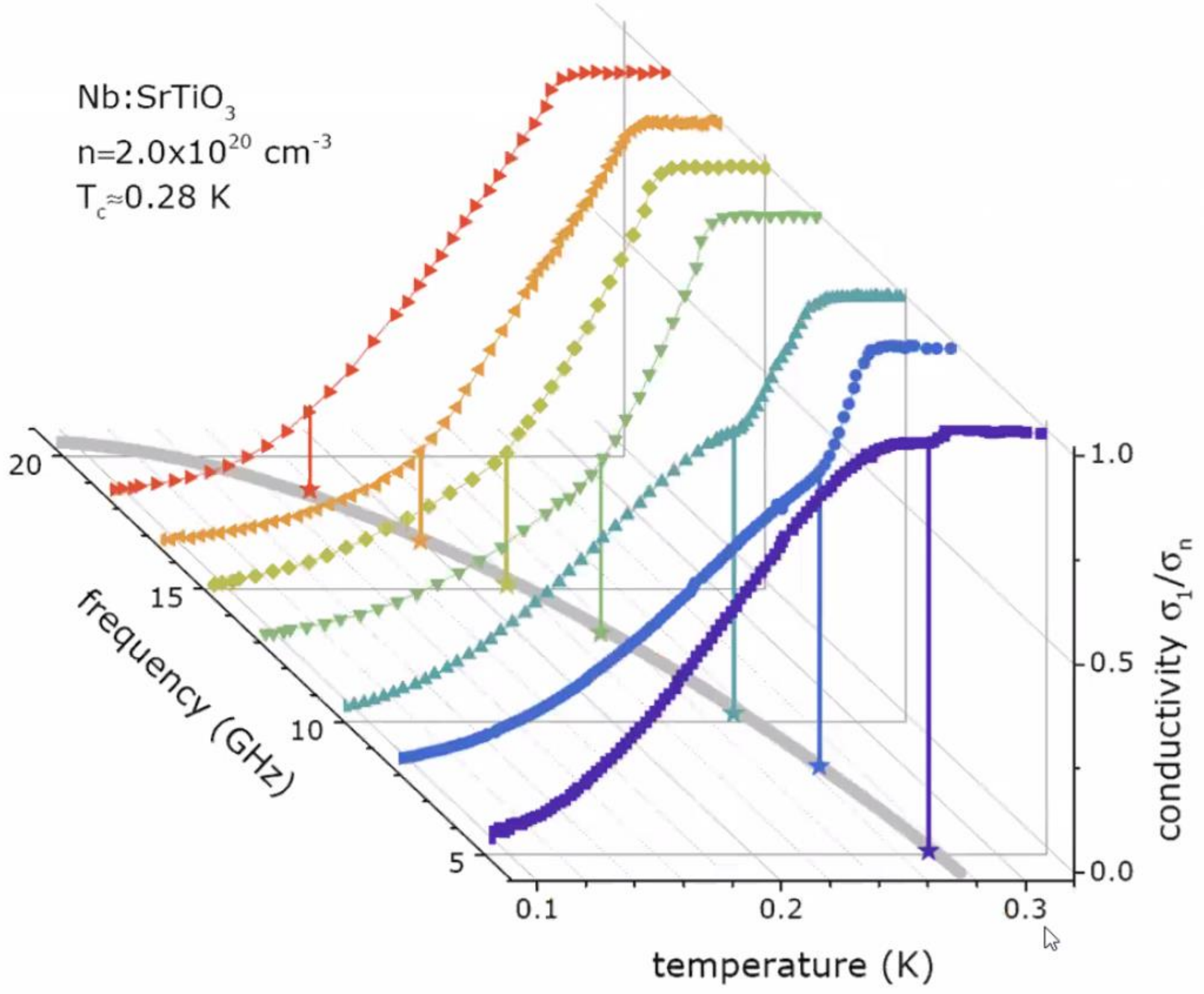

GHz Dielectrics of Undoped $SrTiO_3$ at mK Temperatures

- Superconducting (Nb) coplanar resonator on undoped $SrTiO_3$ in distant flip-chip geometry
- Resonator operation around 1 GHz
- Substantial resonator *Q* at temperatures below 1 K
  - Surprisingly low losses
- Temperature evolution of ε_1:
  - Weak maximum around 3 K
  - Even weaker minimum around 300 mK

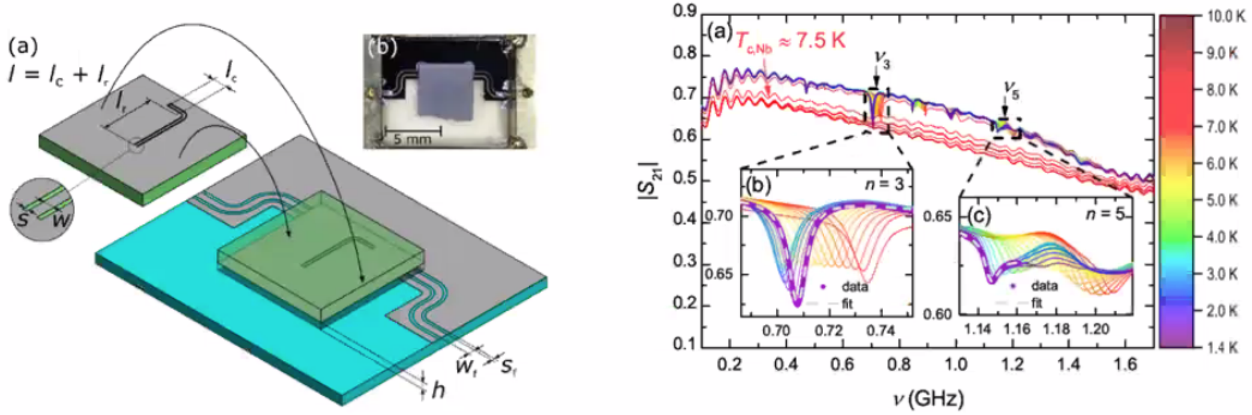

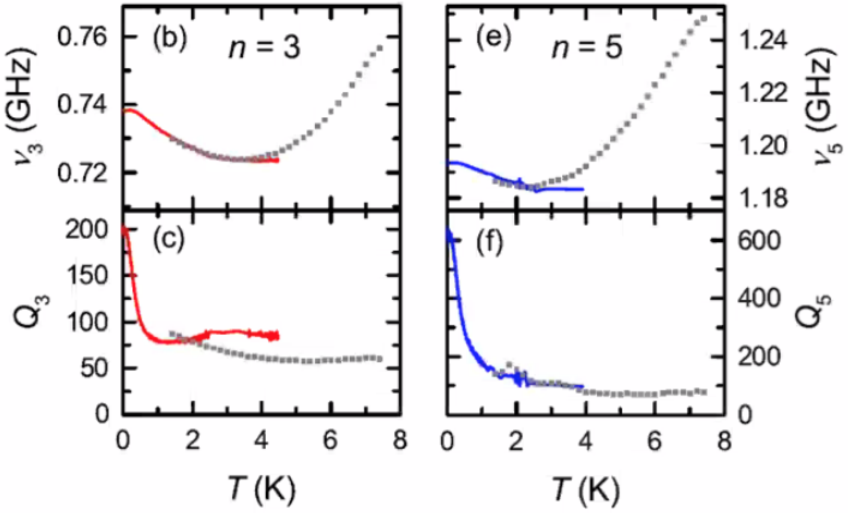

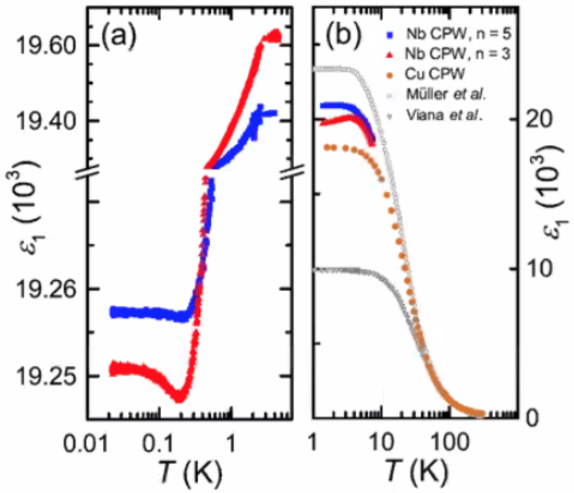

V. T. Engl *et al.*, arXiv:1911.11456

high-Q dielectric cavities for axions

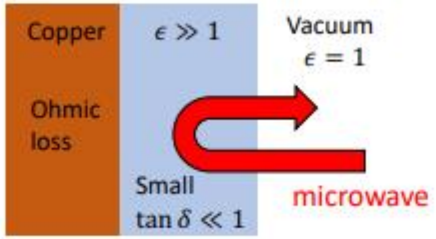

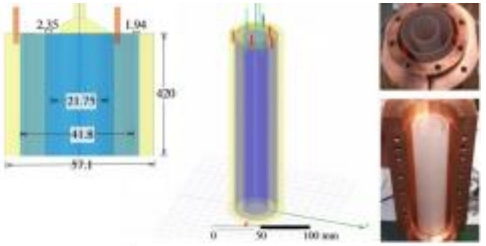

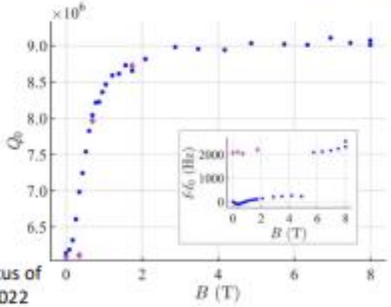

- Dielectric reflects the microwaves to reduce the field strength on the lossy copper surface
- Loss in the dielectric is very low and even lower under magnetic field
- Cryogenic environment at 4 K

Courtesy: Caterina Braggio, "Status of the QUAX experiment" PATRAS2022

MADMAX (DESY)

Courtesy: Antonios Gardikiotis, "Advances in searching for galactic axions with a Dielectric Haloscope"

- Enhance the coherent microwave signal generated on the dielectric surface for dark matter axions
- Around 20 GHz microwaves
- Prototyping with sapphire discs
- 4.2 K operation
- Boost factor is not direct observable unlike Q-factor of cavities → indirect calibration via simulation

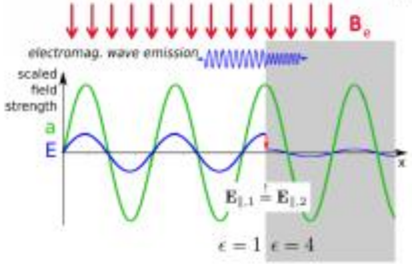

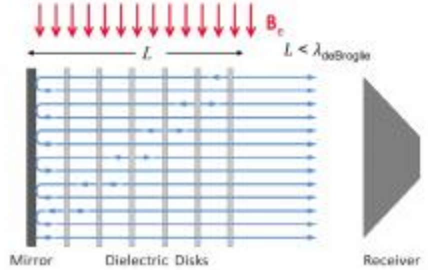

IAXO → solar axion search via X-rays

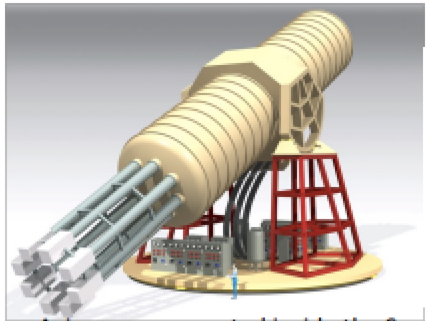

D. Unger *et al* 2021 *JINST* **16** P06006

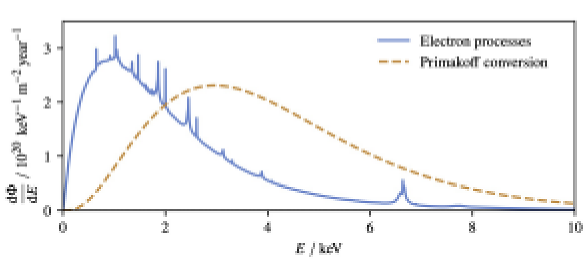

- Axions are generated inside the Sun under its strong magnetic field and photon field
- Axions flying to the Earth is converted to X-ray photons under magnetic field we apply
- Successor of Sumico (PIN photodiode Hamamatsu S3590-06-SPL) & CAST (CCD, micromegas)
- Baseline TPCs equipped with Micromegas → alternative: MMC
- Sensitivity to the axion-photon coupling: $g_{a\gamma} \propto (BL)^{-\frac{1}{2}} \times \left(\frac{\text{BG rate}}{\text{time} \times \text{area}}\right)^{\frac{1}{8}}$

ALPSII → axion generation and detection

Aaron D. Spector PATRAS2023

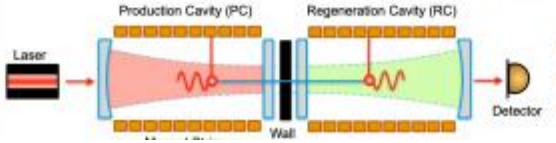

- 1064 nm (1.165 eV) IR photon detection
- Baseline: optical heterodyne
- Alternative: TES

Ferroelectric phase transition and crystal asymmetry monitoring of $SrTiO_3$ using qua: $TE_{m,1,1}$ and quasi $TM_{m,1,1}$ modes

Cite as: J. Appl. Phys. **126**, 104102 (2019); https://doi.org/10.1063/1.5092520
Submitted: 12 February 2019 . Accepted: 18 August 2019 . Published Online: 12 September 2019

M. A. Hosain, J.-M. Le Floch, J. F. Bourhill, J. Krupka, and M. E. Tobar

ABSTRACT

Dielectric spectroscopy of a $SrTiO_3$ single crystal over a broad range of microwave frequency using quasi $TE_{m,1,1}$ and quasi $TM_{m,1,1}$ modes reveals crystal asymmetry from typical measurement of Q-factor, transmission, or frequency characteristics in continuous cooling down to a few Kelvin. The properties of the modes due to the crystal asymmetry are validated by implementing a quasiharmonic phonon approximation. The observed ferroelectric phase transition temperature is around 51 K, and quantum-mechanical stabilization of the paraelectric phase arises below 5 K with very high permittivity. Also, an antiferrodistortive transition was indicated at 105 K. Landau's theory of correlation length supports the observation of an extra-loss term so the transition may be identified near the Q-factor maxima or transmission maxima depending on the other loss terms present in the cavity. Thus, the ferroelectric phase transition with respect to temperature is identified when its extra-loss term causes a discontinuity or deviation in the derivative of the temperature characteristic near the minimum of total cavity loss (maximum Q-factor or maximum transmission temperature characteristic). This temperature is confirmed by transmission amplitude variation of quasi $TE_{2,1,1}$ under 200 V dc electric field showing the existence of the soft-mode. These measurements support a typical polarization model and explicit temperature dependency of the soft-mode incorporating an imaginary frequency.

Published under license by AIP Publishing. https://doi.org/10.1063/1.5092520

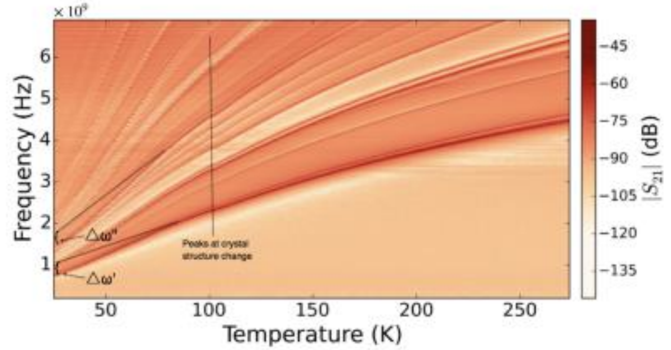

FIG. 2. Frequency shift characteristics of a bunch of dielectric resonance modes of STO under continuous cooling. $\Delta\omega'$ and $\Delta\omega''$ are marked for frequency shift due to soft-mode of FE phase transition.

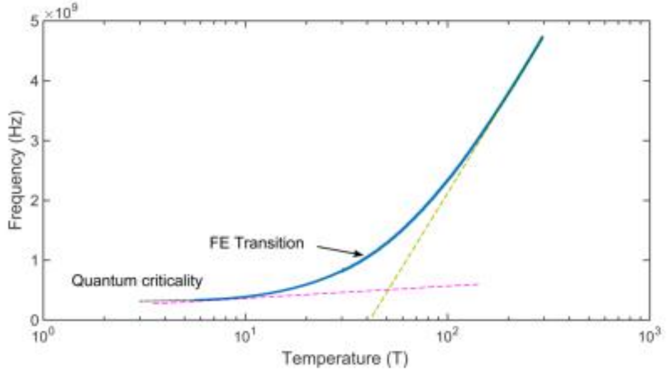

FIG. 4. Frequency shift characteristic of selected mode $TE_{2,1,1}$. The curve turns to a flat region after 5 K.

Supermode Sapphire T=300 K
Courtesy M. Tobar et al

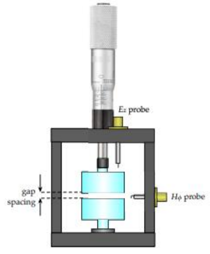

FIG. 1: Proof of concept experimental set up to observe the behaviour of "super modes" as gap spacing is varied between two identical sapphire whispering gallery mode resonators.

Experiment:

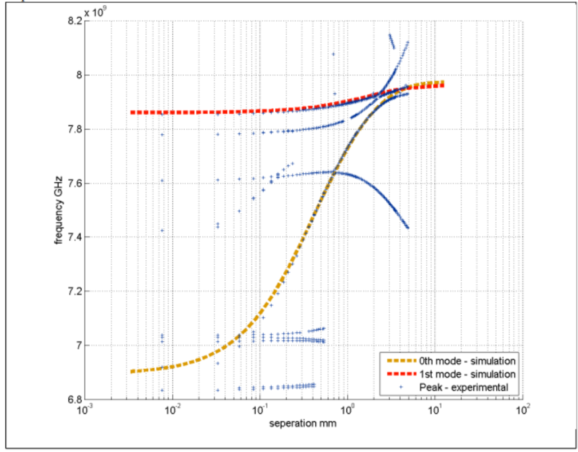

We constructed a cavity with 2 similar small crystals one was z=10.55mm the other z=10.63mm, one crystal was affixed to the floor of the cavity, the second was suspended from an adjustable plunger measured in inches in the ceiling of the cavity. A network analyzer was used to determine the resonant frequencies of the two crystals.

Current activities in collaboration with M. Tobar's group concening SrtiO3 and diamond with NV:

1) Hiqh Q resonators based on supermodes configurations

2) Room temperature Arhanov Bohm effects

3) Doped SrtiO3 Puck measured at milliKenvin

Tesla cavity and dielectric puck modes

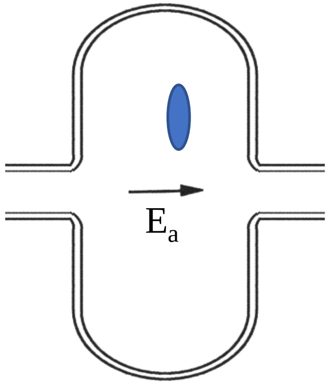

- The goal is to couple the TE mode of the dielectric puck with the TM_{010} mode of the Tesla-shaped accelerating cavity

Shahnam Gorgi Zadeh . et al,
CERN

https://arxiv.org/abs/2410.05831

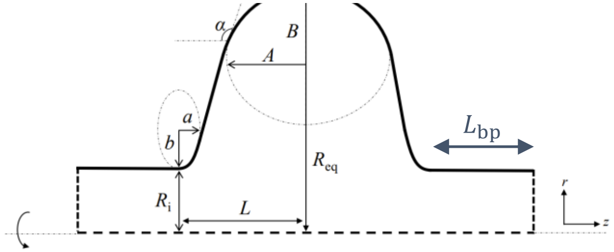

E-field

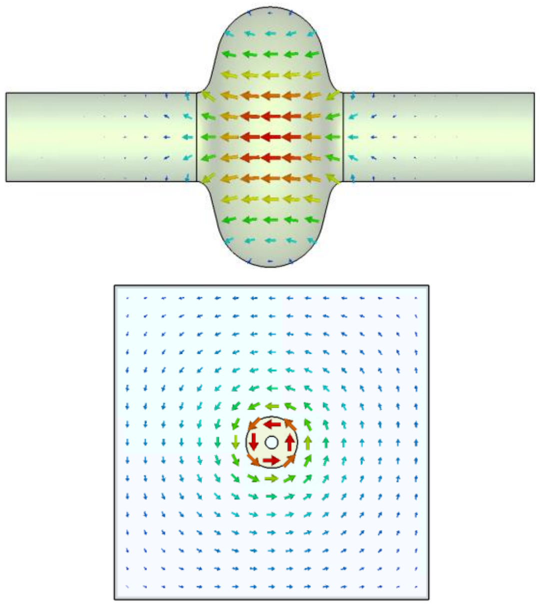

H-field

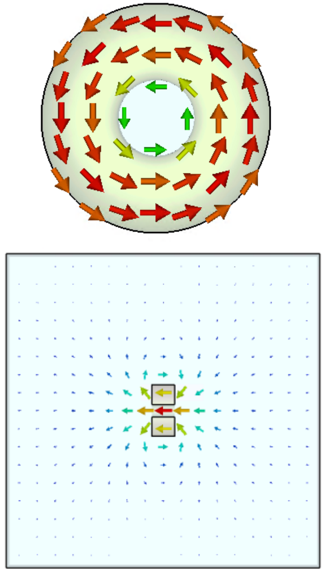

Tesla cavity: $f_{cu} = 1299.977$ MHz, $Q_{cu} = 28885$

Dielectric puck: $f_{puck} = 1101.956$ MHz, $Q_{puck} = 1.01e4$

[redacted]	
A [mm]	42
B [mm]	42
a [mm]	12
b [mm]	19
R_i [mm]	35
L [mm]	57.692
R_{eq} [mm]	102.4496
L_{bp} [mm]	150
f_{cu} [MHz]	1299.977
Q_{cu}	28885
f_{PEC} [MHz]	1300.000

R_{eq} optimized to tune f to 1.3 GHz

Courtesy Walter Venturini CERN

Preliminary measurements of Frequency variations at 1.85 K (VNA) vs time performed by Lorena Ve (2023) (non optimized)

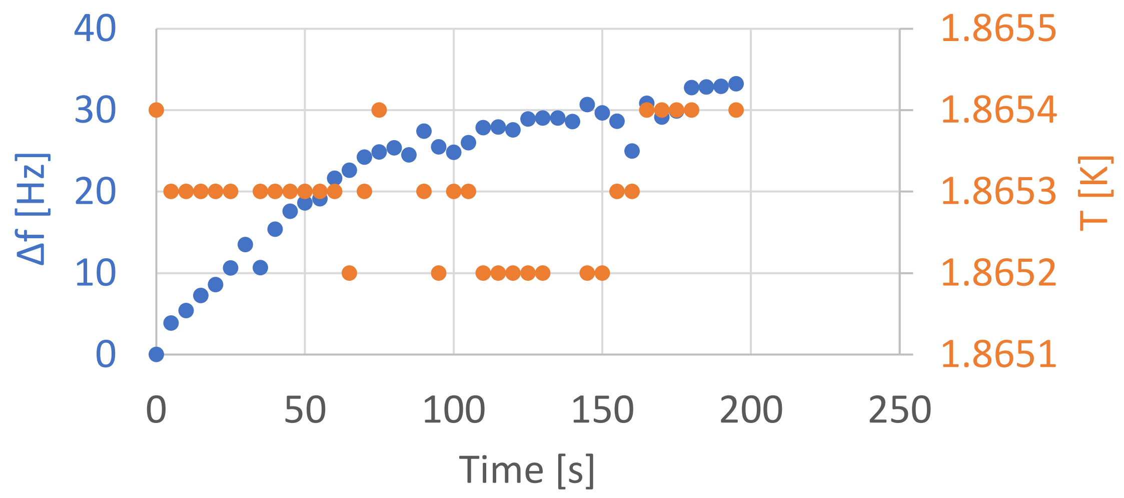

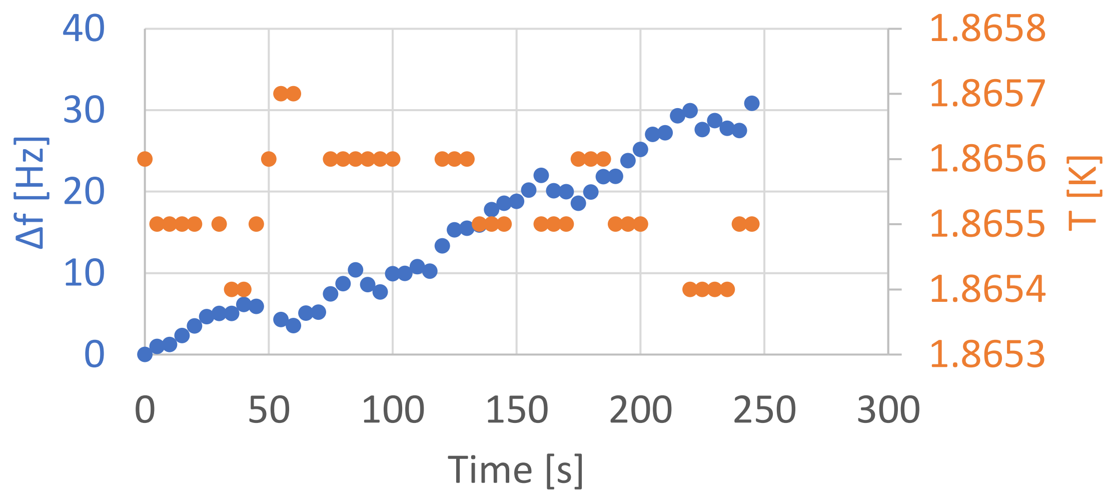

Tests performed connecting 1.3 GHz cavity to VNA:

- Fixed temperature: Helium vapor pressure = 20 mbar (with pressure controller).
- Power: 10 dBm

Dielectric resonators

- **Test of SrtiO3 dielectric resonators**

Shahnam Gorgi Zadeh , et al,
CERN

https://arxiv.org/abs/2410.05831

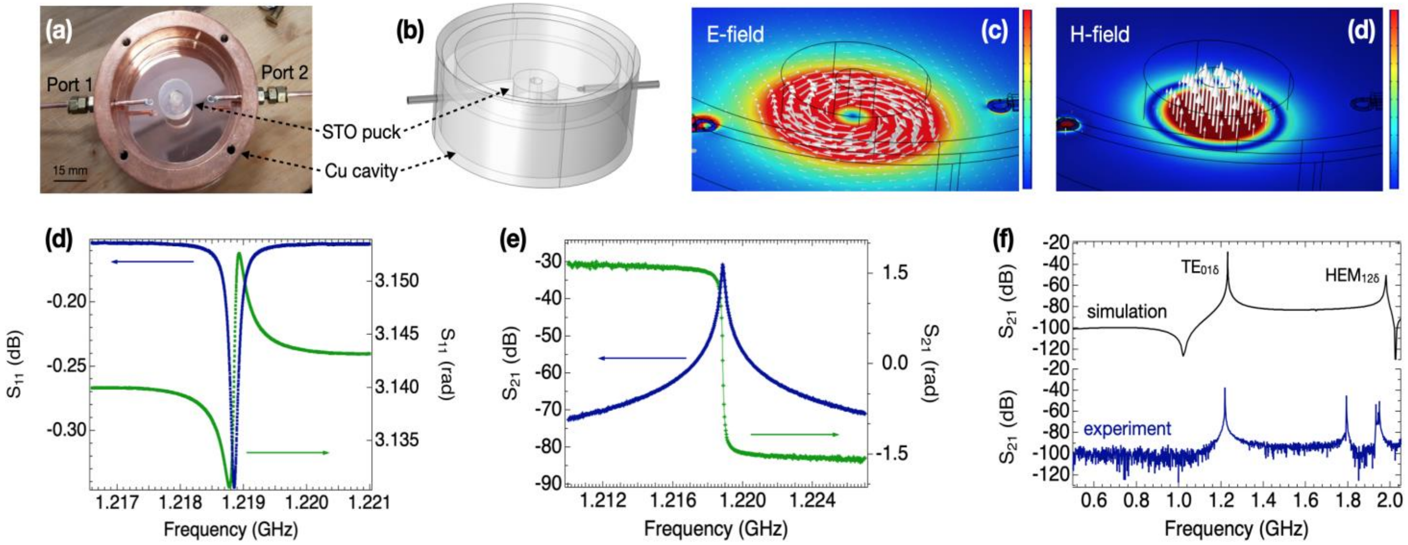

Fundamental mode $TE_{01\delta}$

Permittivity	Loss tangent	Frequency (GHz)
318	1E-04	1.23

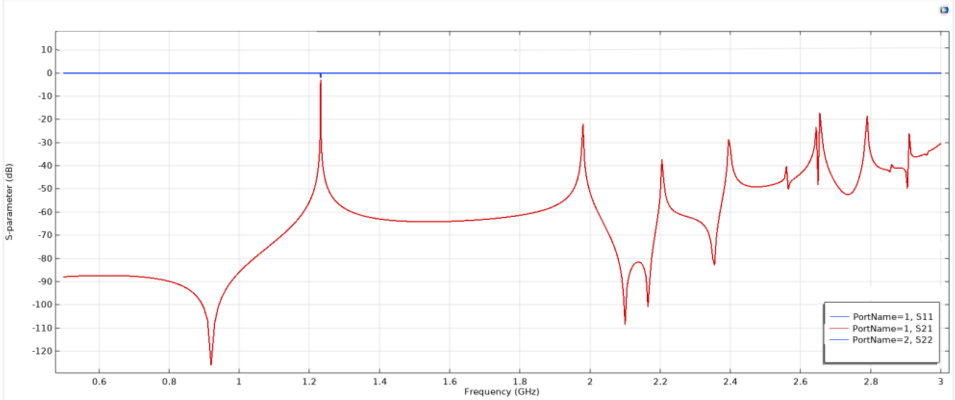

FIG. 1. Characterization of the STO resonator at room temperature. (a) Photograph showing the STO puck and Cu cavity used in the experiments. (b) Sketch of the model used for simulations (COMSOL Multiphysics). The top cap is not shown. (c,d) Simulated distribution of the root-mean-square electric and magnetic field for the TE01δ mode (εr = 318). (d,e) Plots of reflection (S11) and transmission spectra (S21) measured at room temperature (incident power 0 dBm). The amplitude is shown in blue, the phase in green. (f) Comparison between simulated and experimental S21 spectra. The peak at 1.22 GHz is reproduced by the simulated TE01δ mode, while the dip displayed by the simulation at ≈ 1 GHz is below the background transmission of the cavity (−100 dB). The peak at 1.8 GHz is probably related to the hybrid HEM12δ mode, although in this case the simulation shows a mismatch of ≈ 200 MHz.

STO Cu Cavity - **Temperature Comparison**

T-Room Copper Cavity

77 K Copper Cavity

Temperature	Copper Cavity	Dielectric Crystal	Resonant Frequency	Q Factor	Loss	S Parameter
298,15 K 25°C)	**Closed** Cavity	STO	1.207 GHz	7295	-18.35 dB	S21
77 K (-196 °C)	**Closed** Cavity	STO	**478.64 MHz**	**16348**	-20.64 dB	S21

Dielectric resonators SrTi03

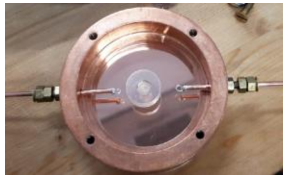

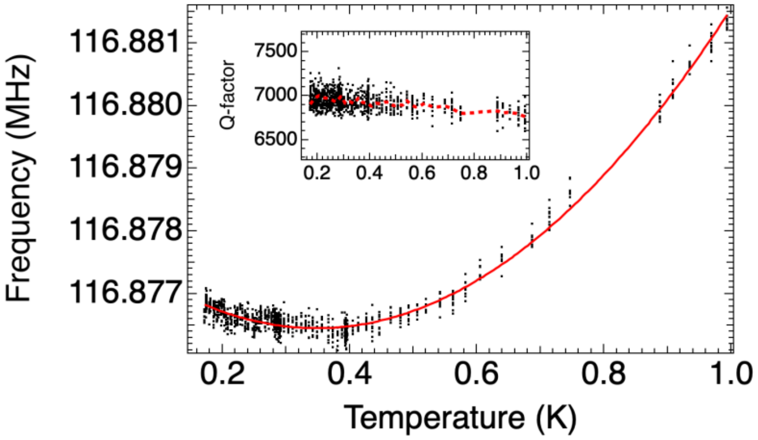

K´

TE$_{01\delta}$, $f_0 = 1.22$ GHz, $Q_L \approx 8000$

mK

TE$_{01\delta}$, $f_0 = 116$ MHz, $Q_L \approx 10000$

ϵ_r(STO) $\approx$ 30000 @ mK

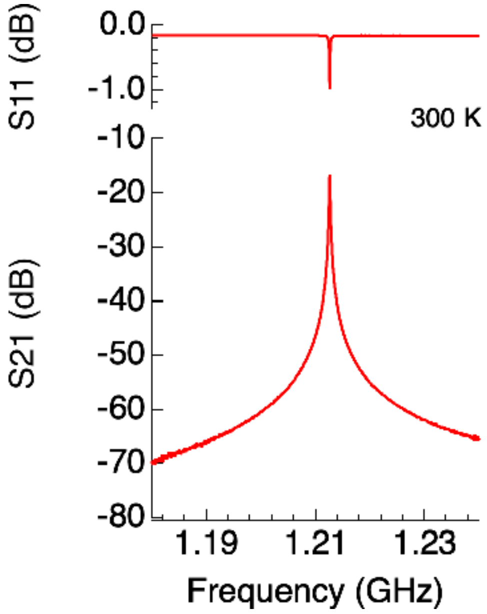

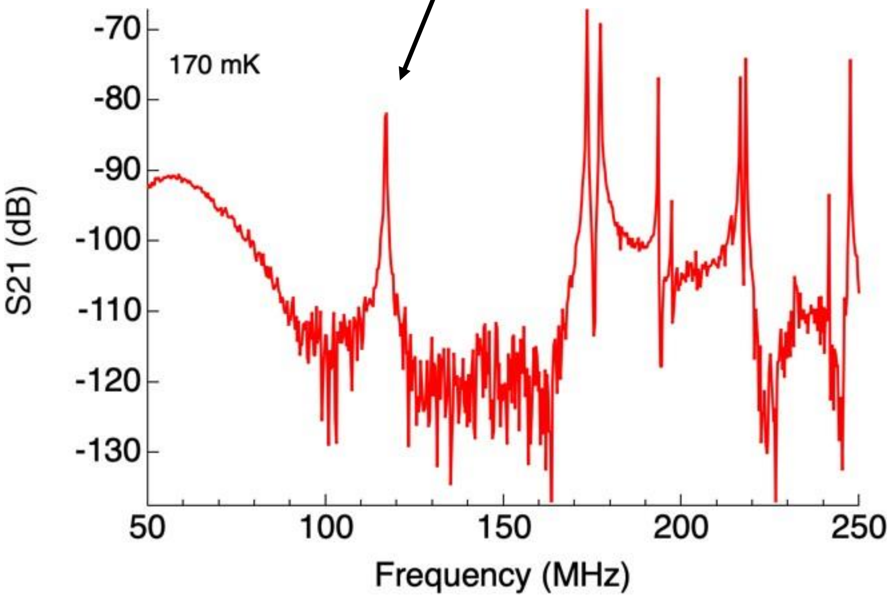

averaged frequency drift: 50 Hz

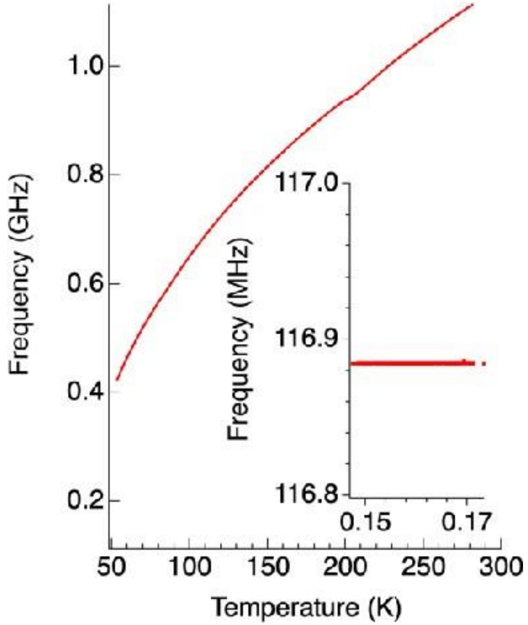

Rutile $TiO2$

The permittivity of TiO2 may be fitted over the whole temperature range by the the same relation for perovskite-type crystals:

$$\boldsymbol{\varepsilon} = A_0 + \frac{C_0}{\frac{1}{2}\,T_1 \coth(\frac{T_1}{2T}) - T_0}$$

Where:
- ***T* is temperature**
- **A_0, C_0, T_1 and T_0 are fitting parameters**

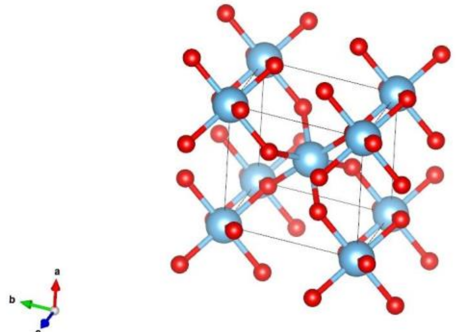

Unit cell of TiO_2.

Structure data from COD-database with COD-code 1534781. (Figure: Mario Mäkinen.)

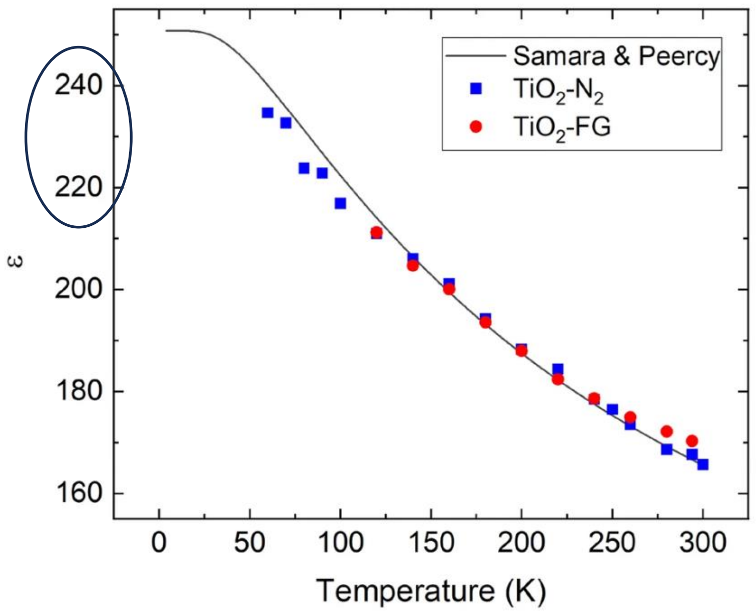

Temperature dependence of the permittivity (ε) of TiO_2

On the permittivity of titanium dioxide – J. Bonkerud (2021)

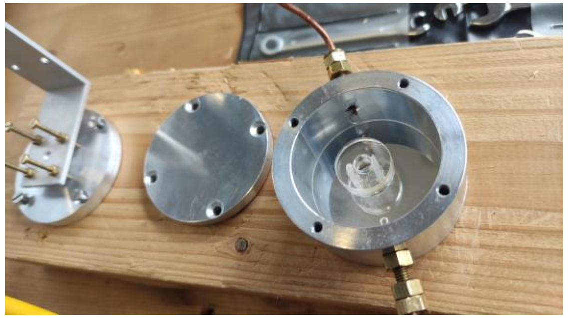

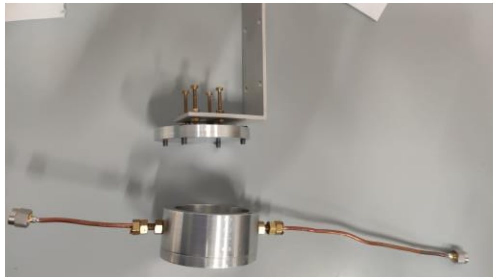

T-Room Al Cavity

Dimensions similar to SrtiO3 Puck

Temperature	Copper Cavity	Dielectric Crystal	Resonant Frequency	Q Factor	Loss	S Parameter
298,15 K 25°C)	**Closed** Cavity	TiO2	2.150 GHz	21490	-21.08 dB	S21
77 K (-196 °C)	**Closed** Cavity	TiO2	1.925 GHz	92949	-16.39 dB	S21

Measurement TiO2 at T= 0.82K

courtesy   Photec Company

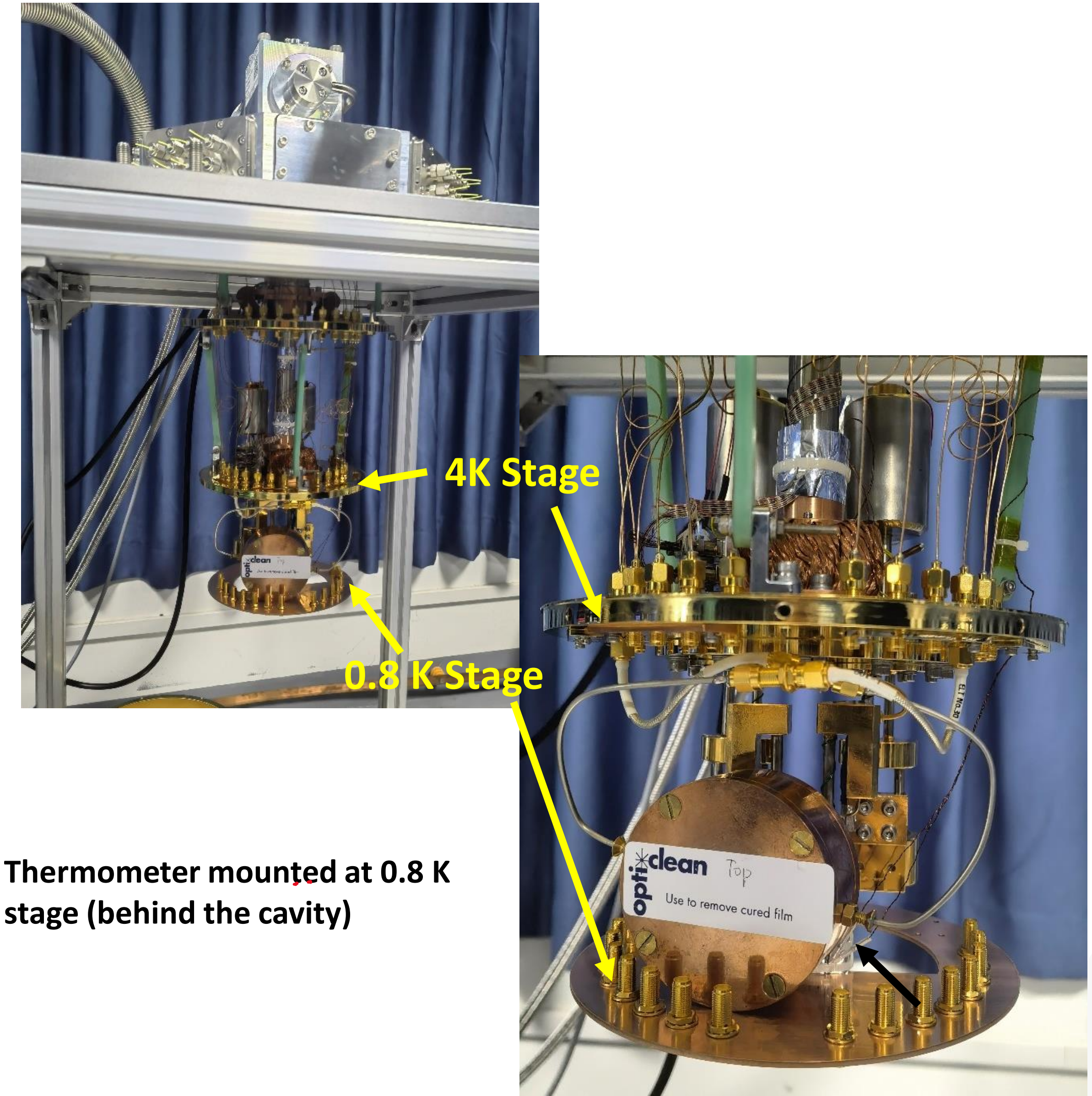

Thermometer mounted at 0.8 K stage (behind the cavity)

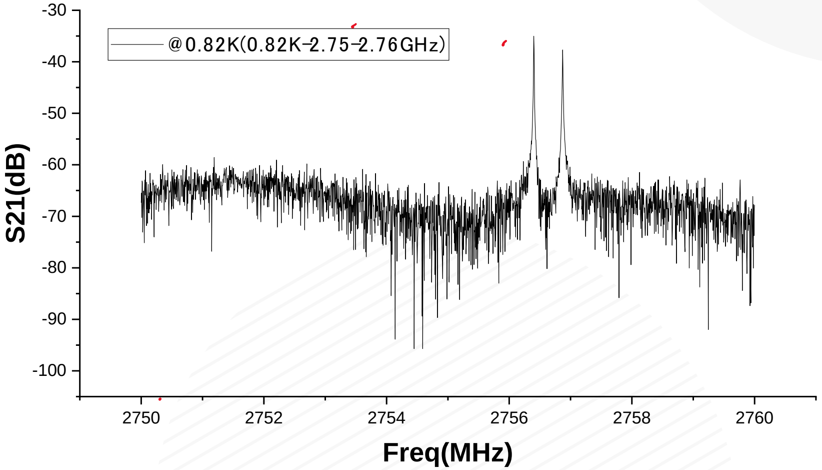

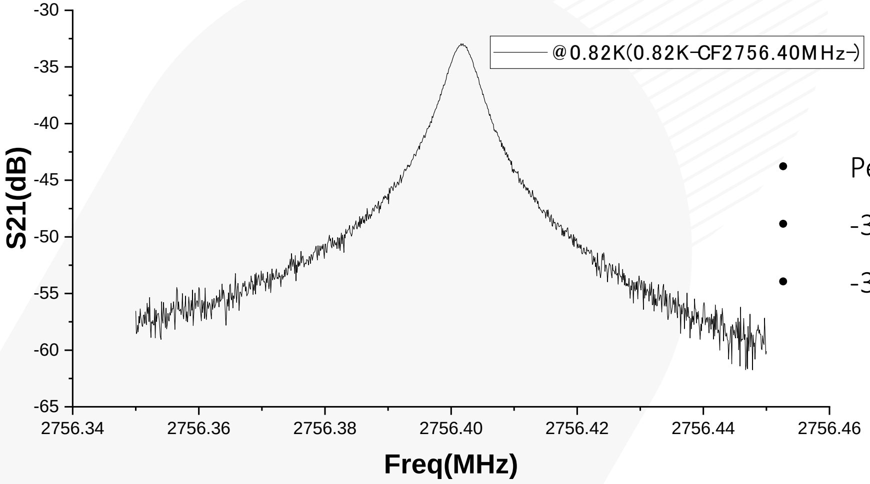

- Peak: 2756.4016 MHz
- -3dB: 2756.3993 MHz
- -3dB: 2756.4042 MHz

Q> 650000

Eigenmode analysis Cu Cavities

- The dielectric material is positioned within the cavity to explore the principle of coupling between the two fundamental modes of the resonators → at around $\varepsilon_r = 230$ strong mode mixing happens
- Tesla mode is identified by its higher R/Q

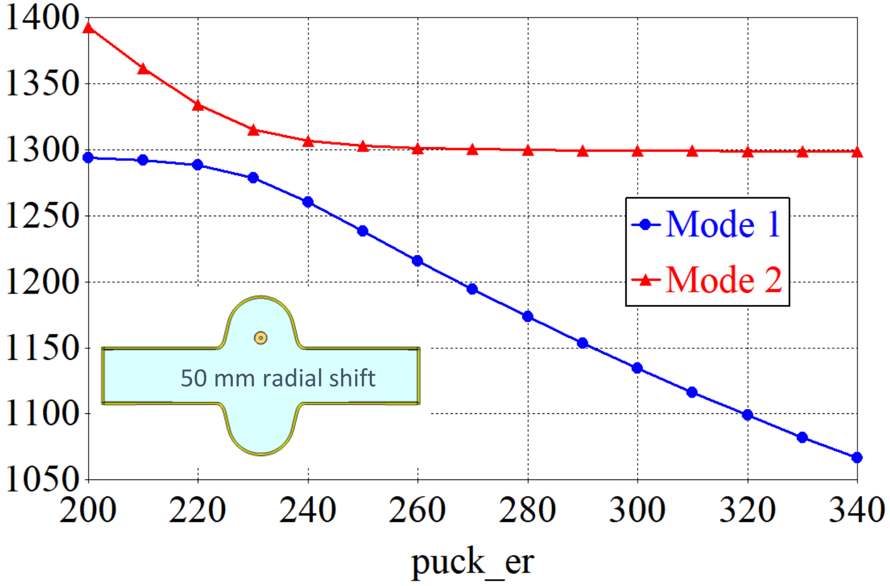

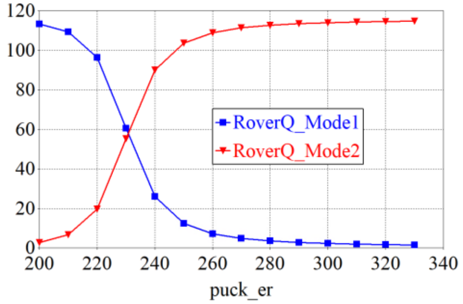

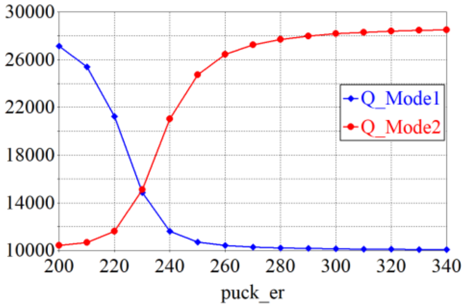

Mode 1:
$f = 1278.494$ MHz
$Q = 1.487e4$
$R/Q = 60.6\ \Omega$

Mode 2:
$f = 1315.208$ MHz
$Q = 1.510e4$
$R/Q = 55.4\ \Omega$

$\varepsilon_r = 230$

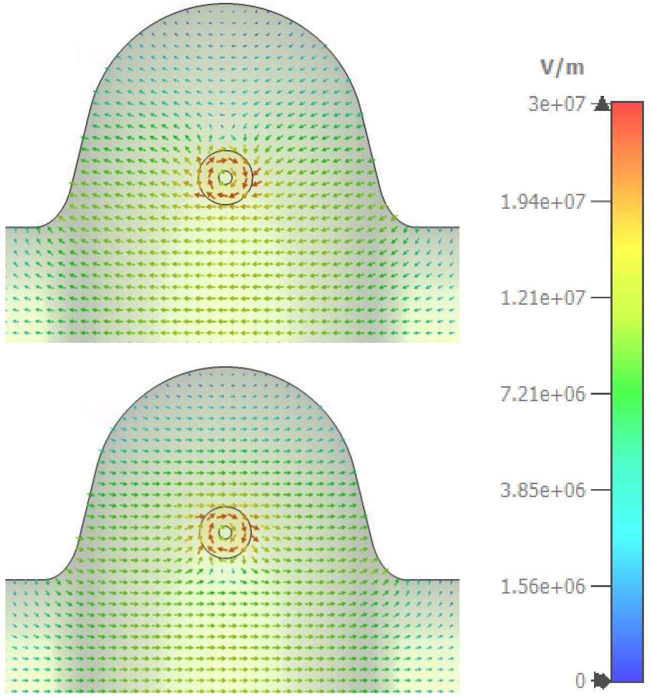

Terminologies

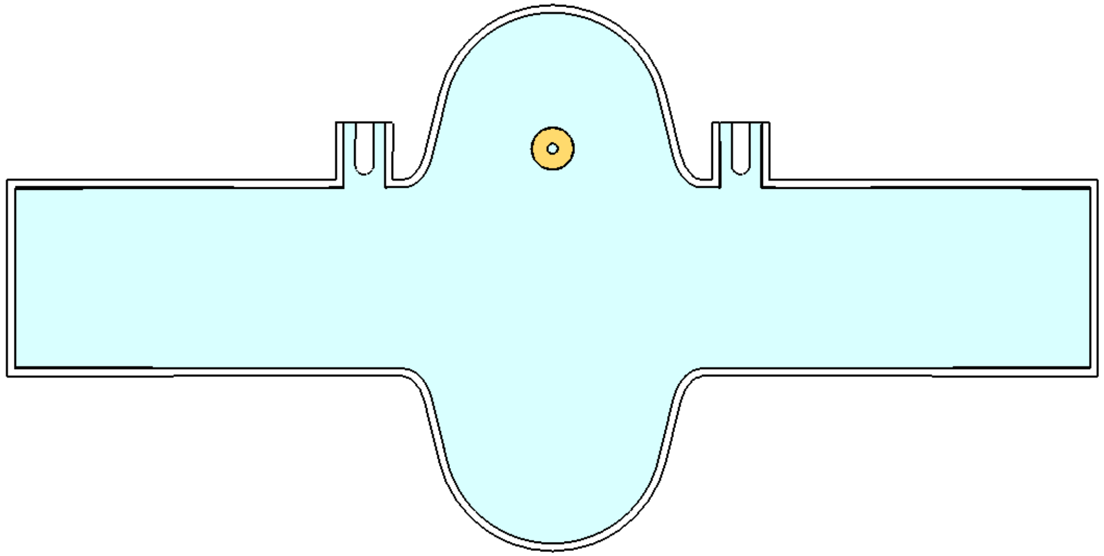

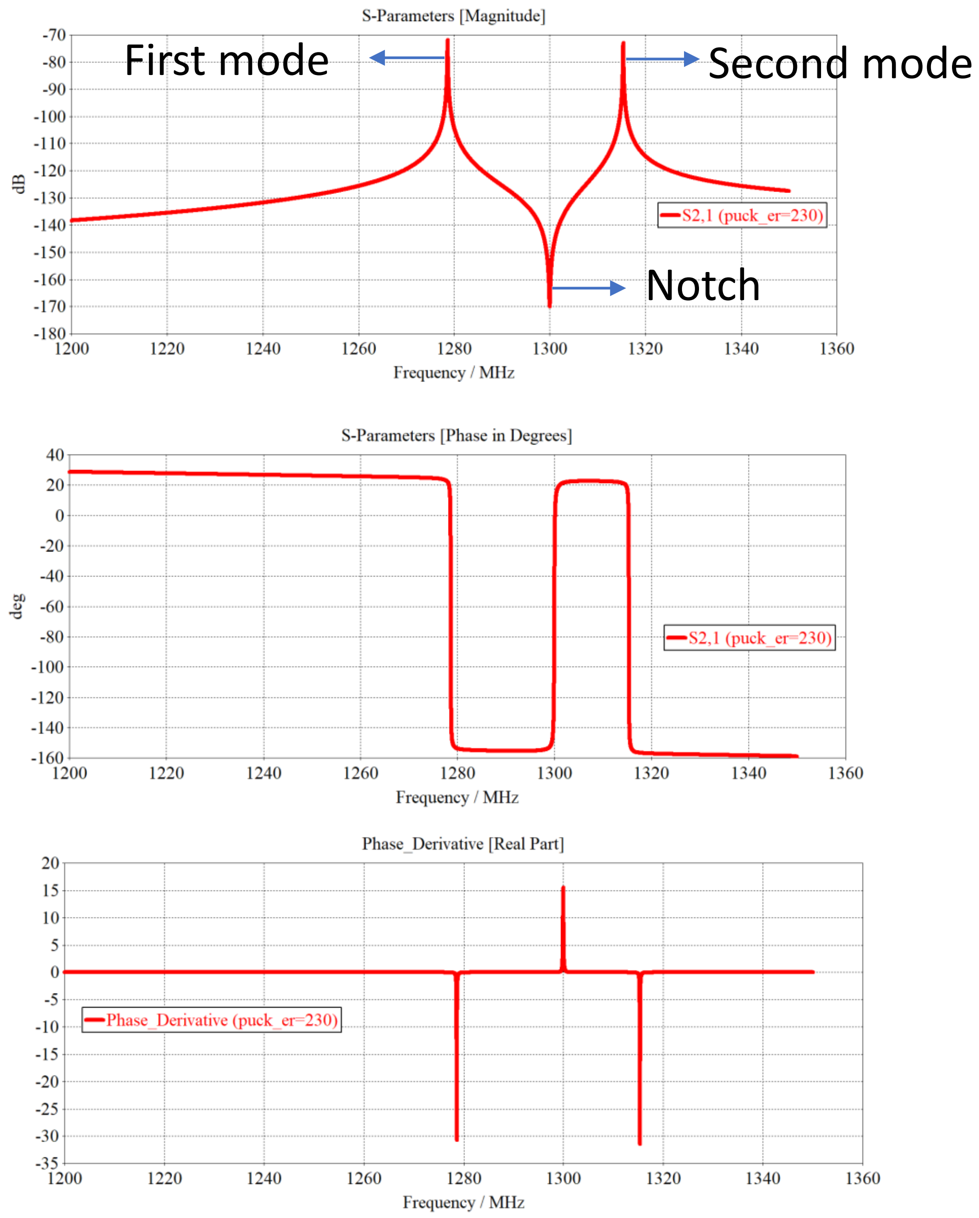

Eigenmode analysis in PEC cavity

- The entire surface of the cavity is changed to PEC and the frequency, quality factor and R/Q of the first two modes are calculated

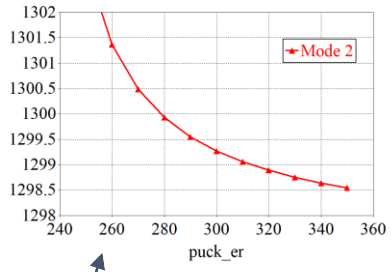

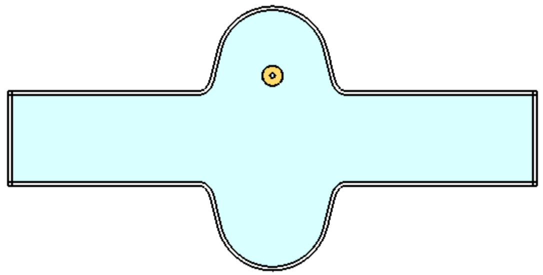

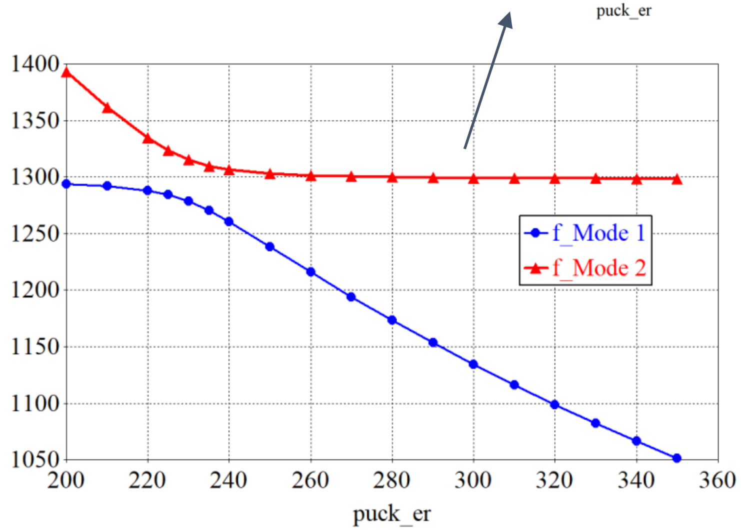

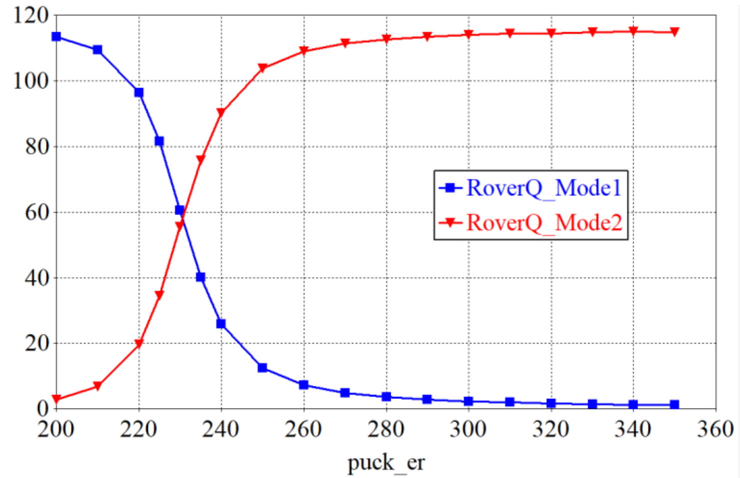

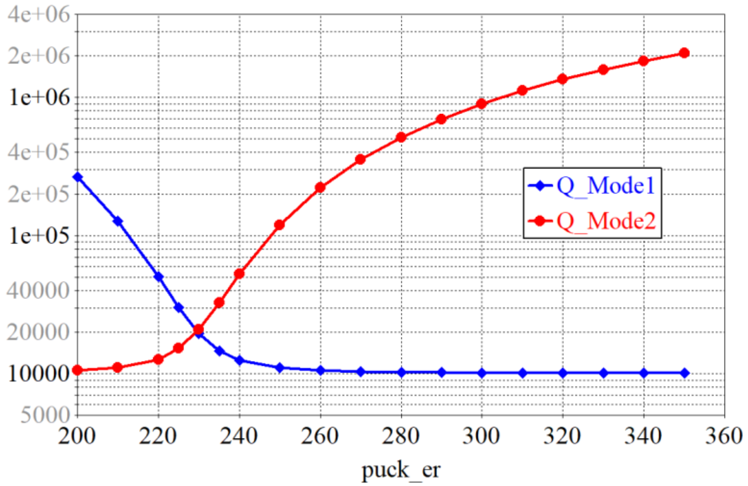

Frequency domain analysis Cu cavities

- Two antennas are positioned on opposite sides of the cavity to examine the transmission between them
- The technical aspects, including the optimal positioning of the dielectric within the cavity, how to secure it, and the suitable excitation scheme, are yet to be explored.

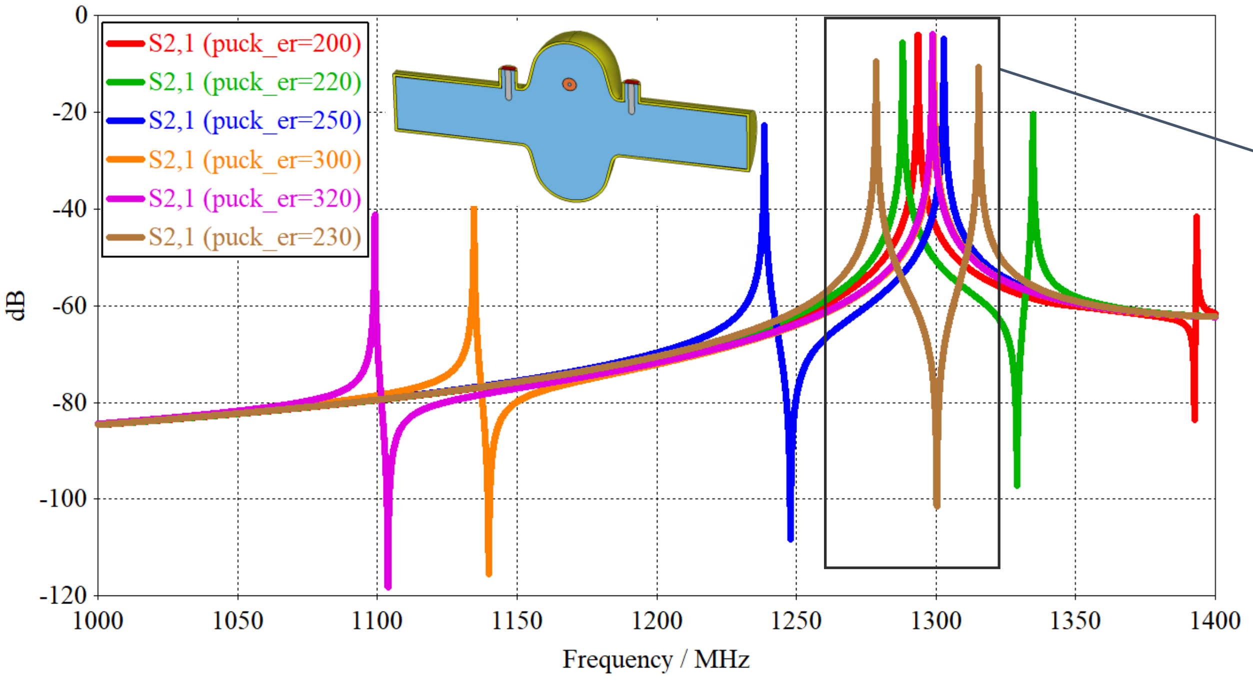

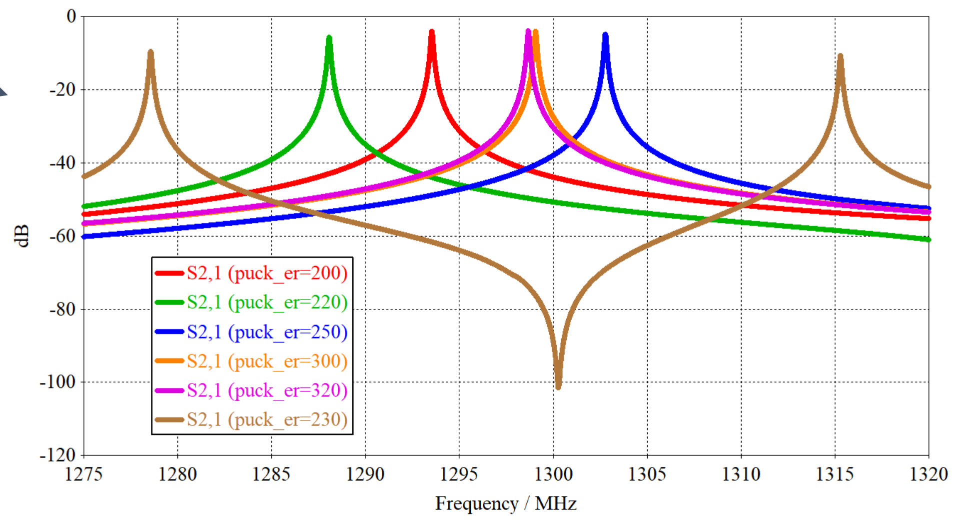

Parameter sweep in $\boldsymbol{\varepsilon_r}$

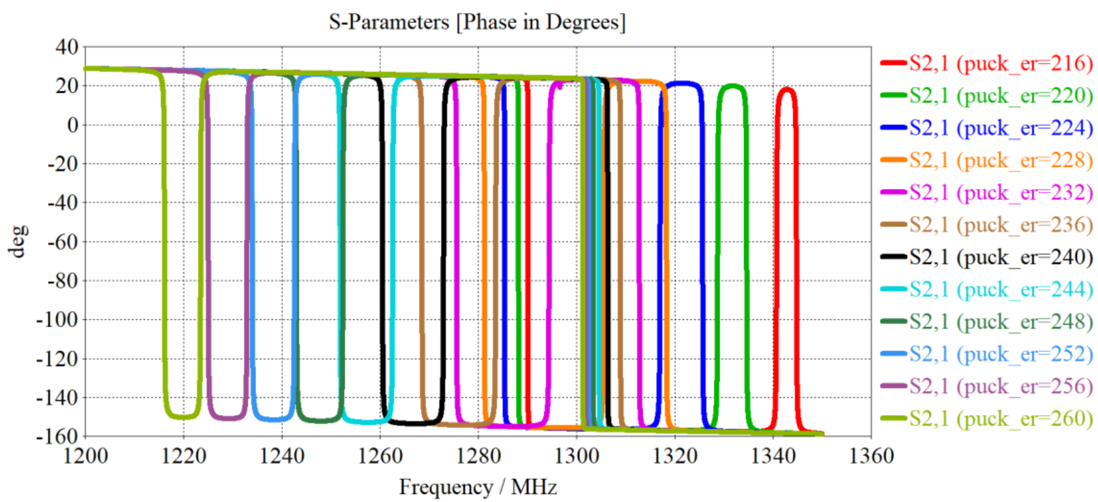

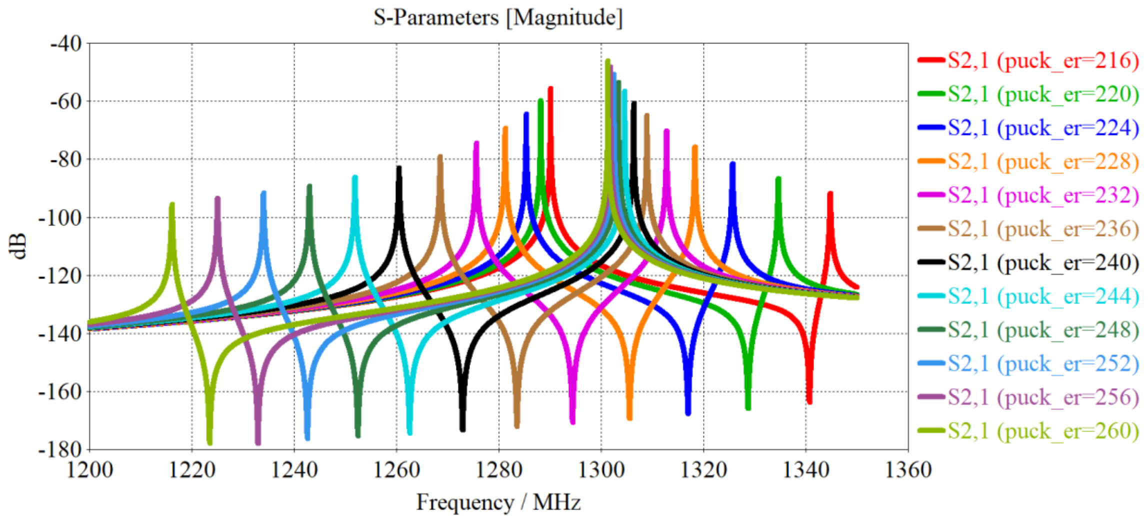

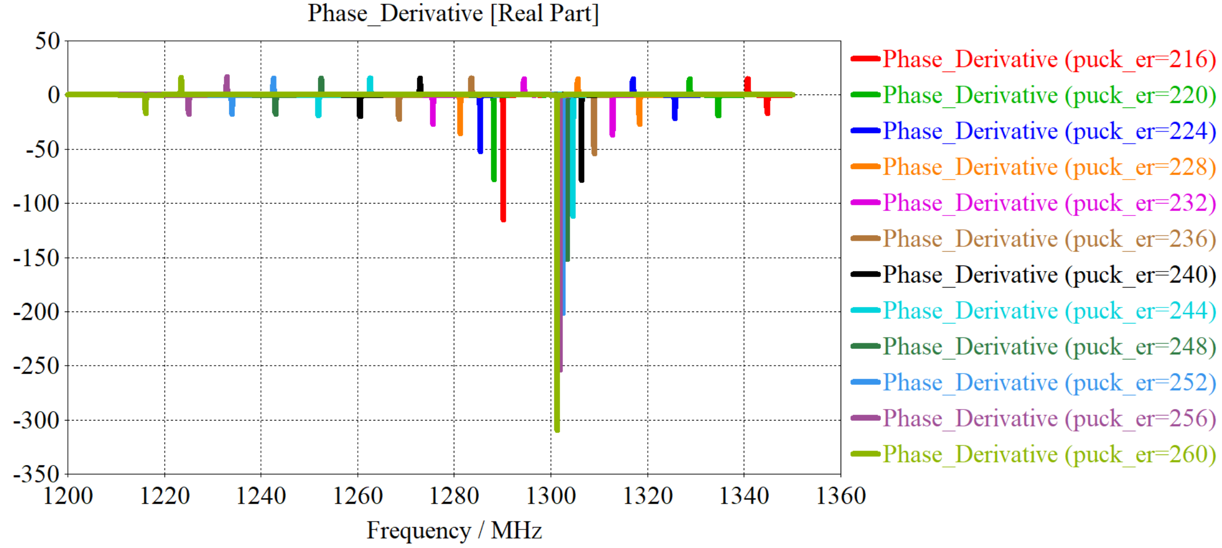

- Phase derivative has high peaks at mode 1, mode 2 and notch frequencies
- Phase derivative amplitude is larger for modes with larger quality factor
- Phase derivative amplitude for the notch seems to have constant amplitude

Frequency sensitivity

Numerical formula:

$$f[\mathrm{GHz}] = \frac{34}{a[\mathrm{mm}]\sqrt{\epsilon_r}}\left(\frac{a}{d} + 3.45\right)$$

(accurate at 2% for $0.5 < a/d < 2$ and $30 < \epsilon_r < 50$)

Black curve data are taken from analytic formula

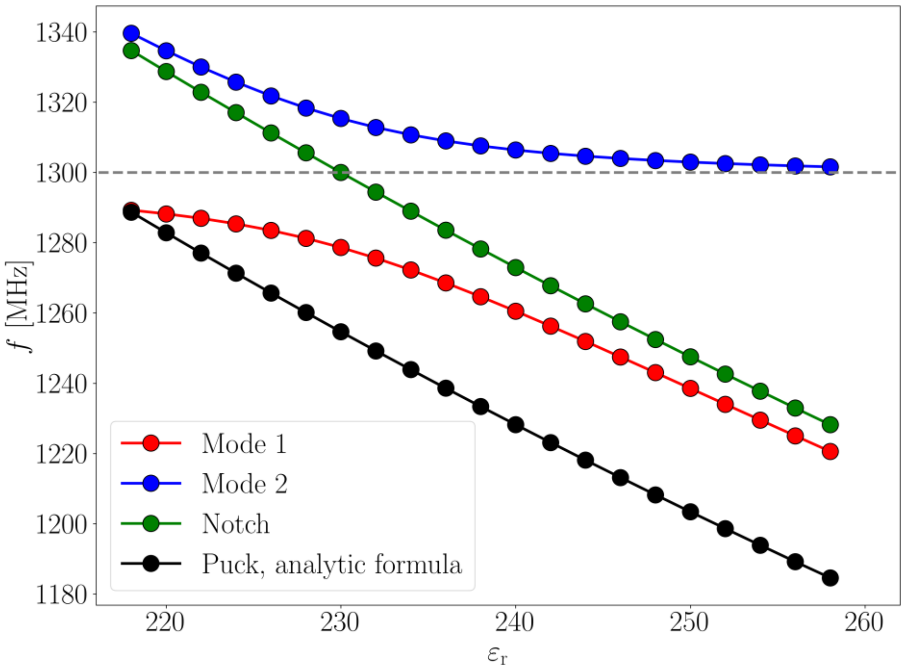

Derivative

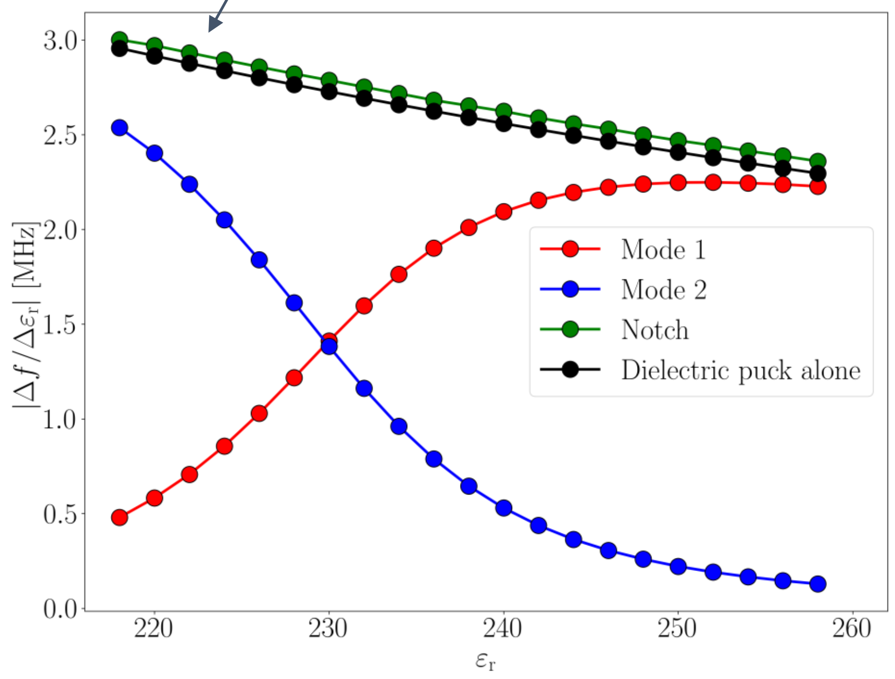

Mode 1 and Mode 2 sensitivities to changes in εr are lower than those of the dielectric puck alone. The notch sensitivity is very similar to that of the dielectric puck alone. **In all cases, no amplification is observed, as the sensitivities cannot exceed those of the dielectric puck alone!!**

Frequency domain analysis in PEC cavity

- The entire surface of the cavity is changed to PEC and the frequency, quality factor and R/Q of the first two modes are calculated

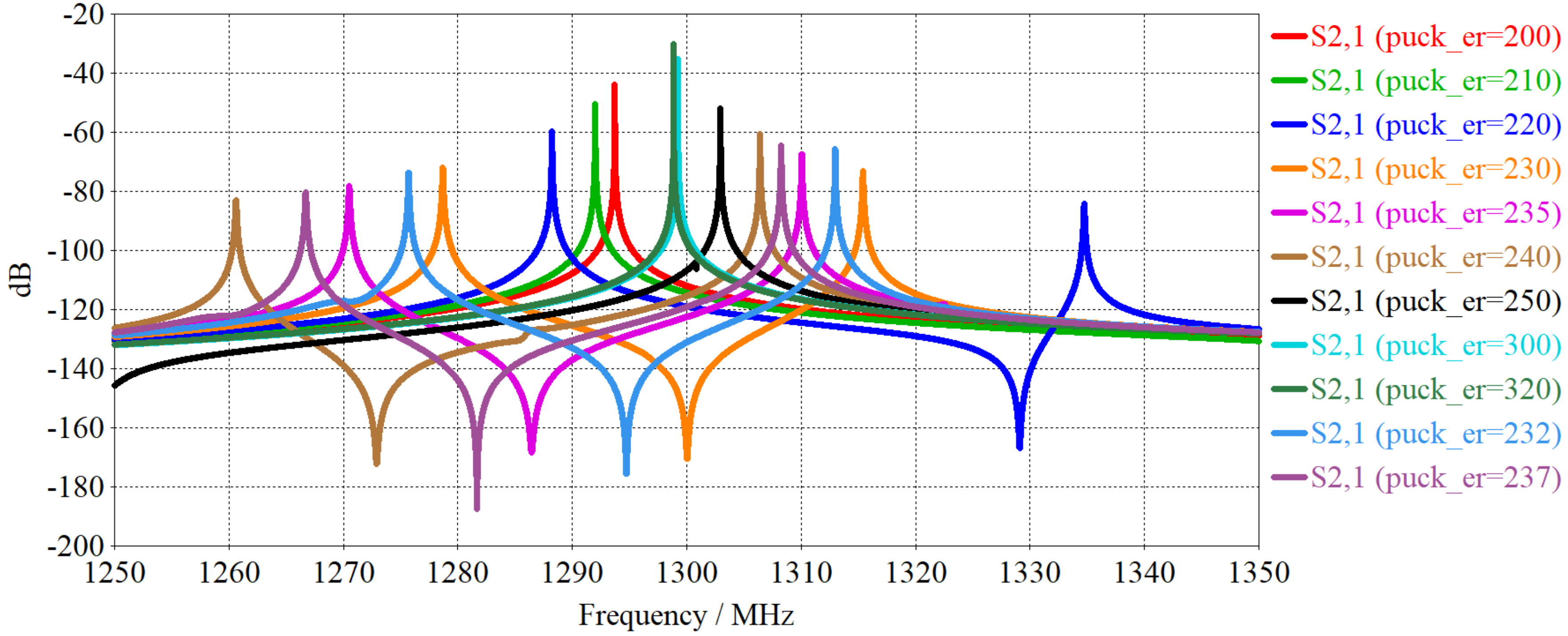

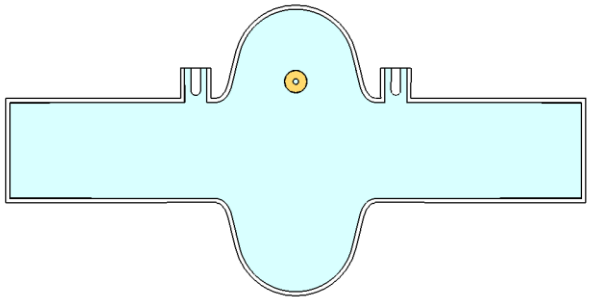

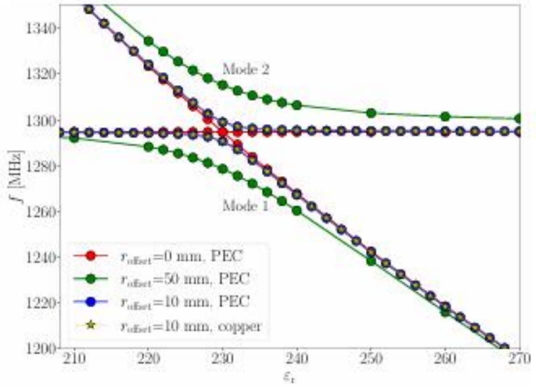

(a)

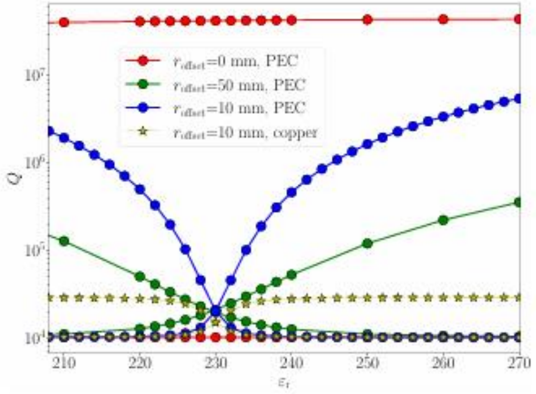

(b)

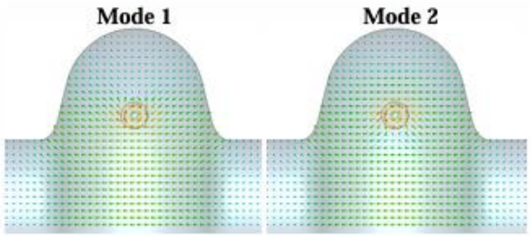

(c)

FIG. 5. Parameter sweep of the dielectric constant (ε_r) of STO and its effect on the frequency and quality factor of the first two modes of the coupled elliptical cavity and STO puck at different radial offset ($r_{\rm offset}$) values. Mode 1 is the mode with the lower frequency. (a) Frequency of the eigenmodes, (b) quality factor of the eigenmodes, and (c) E-field distributions of the two modes at $\varepsilon_r = 230$ and $r_{\rm offset} = 50$ mm.

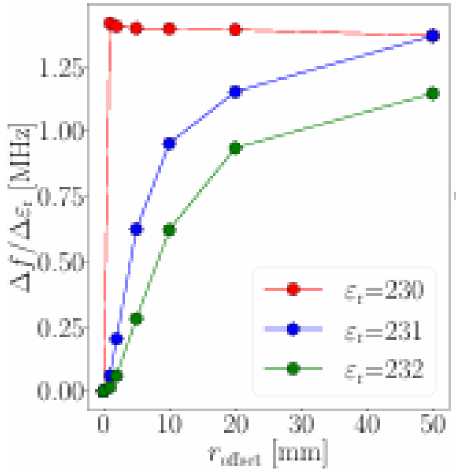

(a)

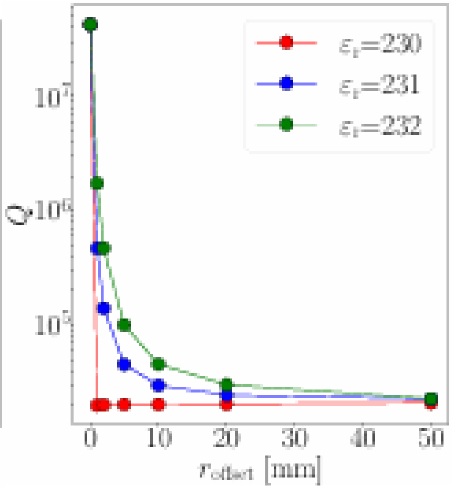

(b)

FIG. 6. Dependency of the frequency sensitivity (a) and quality factor (b) of the elliptical cavity-dominant mode with respect to $r_{\rm offset}$ at different values of ε_r.

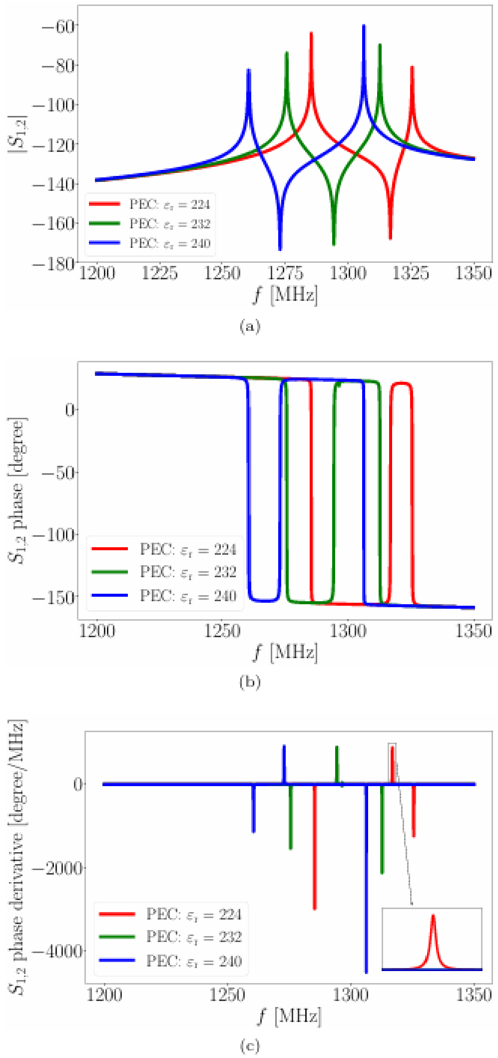

FIG. 7. S-parameters of the excitation scheme shown in Fig. 4 at different ε_r and $r_{\rm offset} = 50\,\rm mm$ for a PEC cavity. (a) Magnitude of $S_{1,2}$, (b) Phase (φ) of $S_{1,2}$, and (c) Phase derivative ($\mathrm{d}\varphi/\mathrm{d}f$) of $S_{1,2}$. Varying ε_r shifts the resonance frequencies of the two peaks and the notch. The phase derivative is linked to the quality factor, with higher amplitude for the mode with the larger Q-factor, and shows minimal change at the notch as ε_r varies.

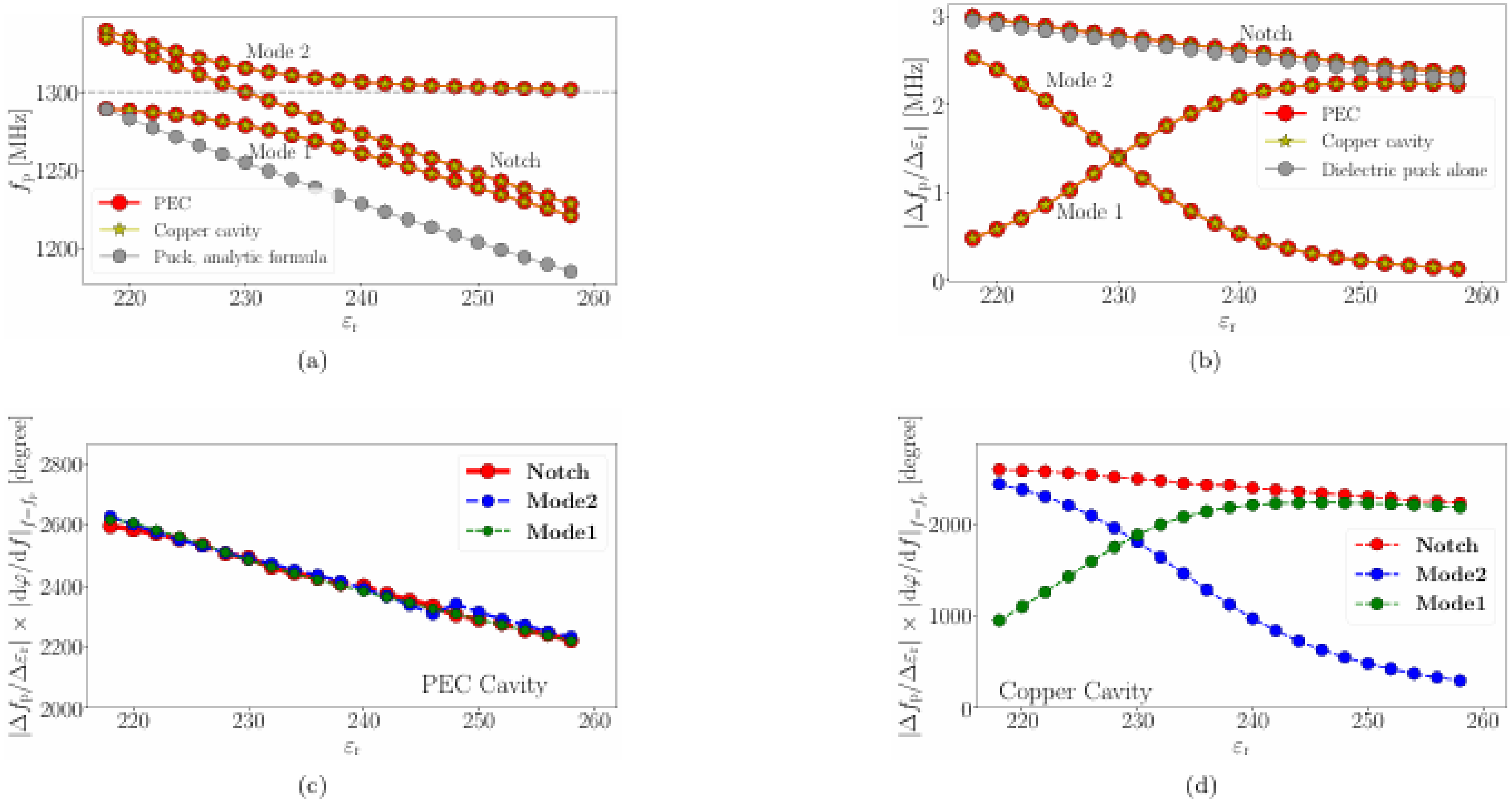

FIG. 8. Analysis of the S-parameters shown in Fig. 7. (a) Frequencies of the first and second peaks, as well as the notch, of the $|S_{1,2}|$ curves shown in Fig. 7(a). (b) Derivative of the curves from (a). (c) and (d) show the curves in (b) multiplied by the phase derivative at $f = f_{\rm p}$ (from Fig. 7(c)), for a PEC cavity and a copper cavity, respectively. Mode 1 and Mode 2 correspond to the frequencies of the first and second peaks of the $|S_{1,2}|$ curves, respectively, and the notch corresponds to the frequency of the dip between these two peaks. The frequency of the puck alone and its derivative calculated by the semi-analytic formula is also shown in (a) and (b). The product of frequency sensitivity and the maximum phase derivative is almost equal at the notch for both the PEC and copper cavities (red curves in (c) and (d)). However, for modes 1 and 2, it is smaller in the copper cavity compared to the PEC cavity near $\varepsilon_{\rm r}$ of 230, where the coupling is at its maximum.

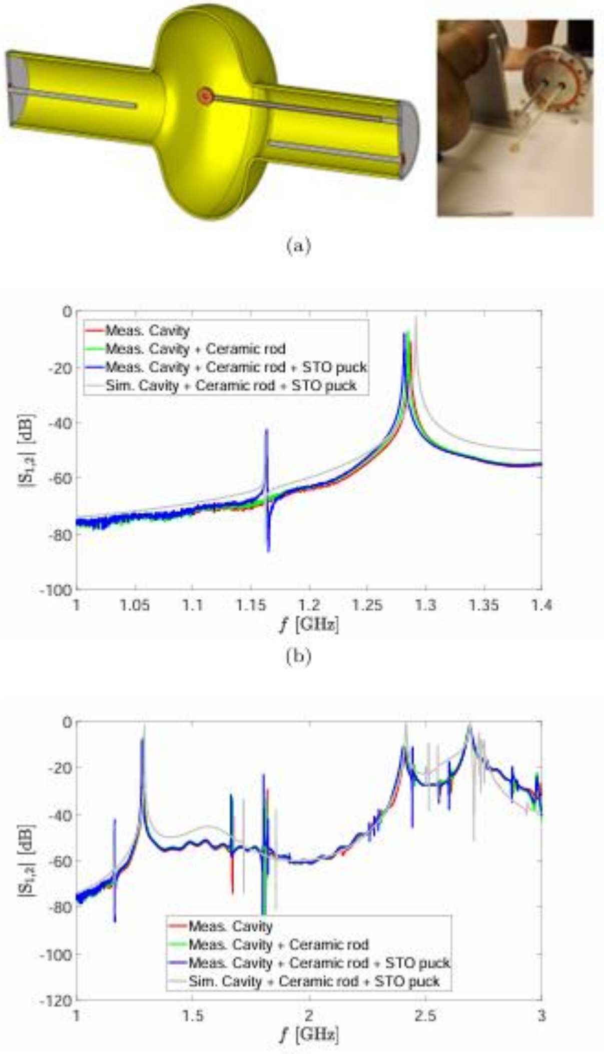

FIG. 9. The measurement setup (a) and measurement results of the coupled elliptical cavity with the STO puck over a narrow frequency range (b) and a wide frequency range(c). The STO puck is fixed to the flange via a long ceramicrod at roffset=19 mm. Two long antennas were used for the S2,1 measurement: one at the flange center and the other at roffset=-19 mm. Note that the elliptical cavity used for the measurements had a slightly different shape than the one used for the simulations, causing a small change of the resonance modes of the cavity. An εr of 300 is assumed in the simulation.

Anyway, if we trust Gallop's numbers

$$\Delta\epsilon = \frac{d\epsilon}{dT}\Delta T = 7\times10^3\Delta T$$

100 keV X-ray: $\Delta T = \sim0.1\ \mu\text{K} \rightarrow \Delta\epsilon = 7\times10^{-4}$
1 eV IR photon: $\Delta T \sim 0.1\ \text{pK} \rightarrow \Delta\epsilon = 7\times10^{-10}$
1.3 GHz RF photon: $\Delta T = 5.5\times10^{-18}\ \text{K} \rightarrow \Delta\epsilon = 3.9\times10^{-14}$

$\epsilon \rightarrow \Delta f$ by Shahnam

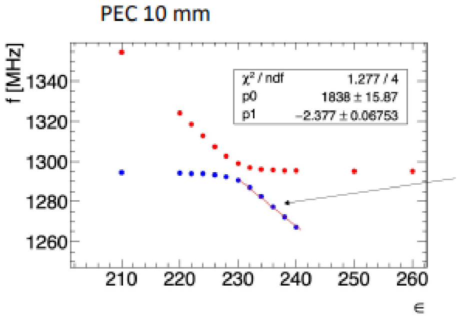

$$\frac{df}{d\epsilon} = -2.377\ \text{MHz}$$

$$f(\epsilon \circ T)$$

$$\Delta f\,[\text{Hz}] = \frac{df}{d\epsilon}\frac{d\epsilon}{dT}\Delta T = -2.377\times10^6\times7\times10^3\Delta T = 1.7\times10^{10}\ \Delta T\ [K]$$

100 keV X-ray: $\Delta T = \sim0.1\ \mu\text{K} \rightarrow \Delta f = 1.7\ \text{kHz}$
1 eV IR photon: $\Delta T \sim 0.1\ \text{pK} \rightarrow \Delta f = 1.7\ \text{mHz}$
1.3 GHz RF photon: $\Delta T = 5.5\times10^{-18}\ \text{K} \rightarrow \Delta f \sim 1\ \text{nHz}$

The stabilized RF cavities can resolve probably 10 Hz
→ $dE_{min} = 590$ eV
→ This is a typical energy of soft X-ray (challenging!)
→ Realistic goal of this technology is soft X-ray counting

Conclusions

- We have studied the hybrid system composed by a high-Q TESLA-shaped elliptical cavity and STO resonator, and investigated the effect of parameters, such as STO permittivity, puck dimensions and position within the cavity, that govern the coupling between the electromagnetic modes.

-Finite-element simulations show that the hybrid system offers great versatility to tune the coupling strength and achieve the strong coupling regime.

-These results are supported by test measurements carried out at room temperature using a copper cavity and a STO puck, and by the low temperature characterization of the STO resonator, which shows resonant frequency of 0.1 GHz and Q-factor of 10000 and er =30000 at0.16 K.

-The hybrid system show potential for the realization of microwave sensors in which the sensitivity of the STO puck to selected physical quantities is exploited as the active element, while frequency or phase measurements on the high-Q cavity are used to efficiently detect such changes.

-In particular, the application of the hybrid system in bolometers exploiting the temperature dependence of the STO permittivity has been discussed.

-Our results are useful to design dedicated experiments at low temperature allowing the direct test of sensitivity and tunability of the proposed hybrid system in high precision frequency-domain measurements.

We thank Giovanni, Romano, Fritz Casper, Sergio Calatroni, Akira Miyazaki, Walter Venturini, Alick Mcpherson, Giovanni Carugno, Marco Affronte , Micheal Tobar